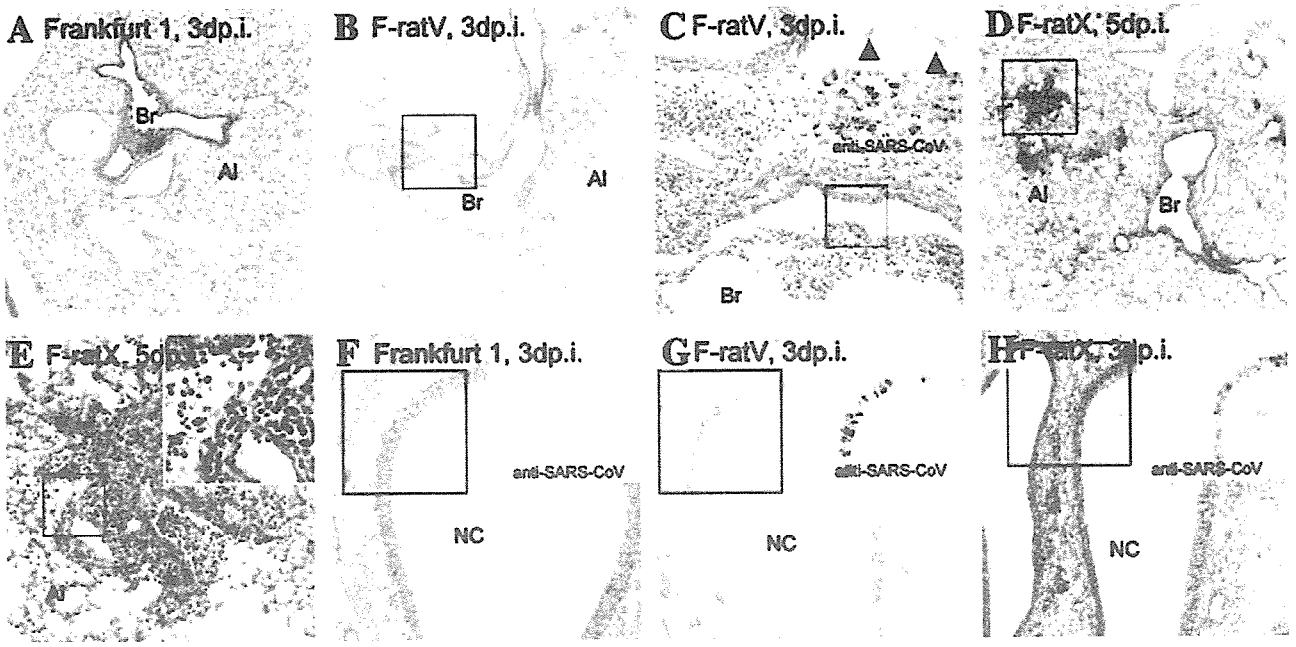

FIG. 2. Histopathologies of lung (A to E) and nasal cavity (F to H) in young F344 rats (4-week-old females; $n = 3$) after intranasal inoculation with serially passaged virus. Br, bronchi; Al, alveoli; NC, nasal cavity. (A) No inflammatory infiltrates in lung after inoculation with the Frankfurt 1 isolate were observed on day 3 p.i. (hematoxylin and eosin staining) (magnification, ×10). (B and C) Slight inflammatory reactions around bronchioles were observed in F344 rats after intranasal inoculation with five-times-serially-passaged Frankfurt 1 strain F-ratV on day 3 p.i. (C) Extensive cellular debris in bronchioles comprised of necrotic epithelia and inflammatory cells (magnification, ×50). Immunohistochemical staining using SARS-CoV-specific antibody detected virus antigen-positive cells in bronchioles and epithelial cells (C, inset) (immunohistochemistry) (magnification, ×100). (D and E) Expanded inflammatory reactions around bronchioles and the alveolar area were observed in F344 rats after inoculation with 10-times-serially-passaged Frankfurt 1 strain F-ratX on day 5 (magnifications, ×10 [D], ×50 [E], and ×100 [inset]) p.i. Small hemorrhages (*) and infiltration of lymphocytes were observed in peribronchiolar alveoli (E, inset). (F) No inflammatory reactions or virus antigen-positive cells were observed in the nasal cavity after inoculation with the Frankfurt 1 isolate on day 3 p.i. (G) Degenerated virus antigen-positive epithelial cells were observed in the nasal cavity after inoculation with F-ratV on day 3 p.i. (H) Massive inflammatory reactions and virus antigen-positive cells were observed in the nasal cavity after inoculation with F-ratX on day 3 p.i. (magnification, ×25 [F to H]).

respiratory tract of young F344 rats were higher than that seen with the original Frankfurt 1 isolate (Fig. 2 and Table 1). Young F344 rats inoculated with the original Frankfurt 1 isolate showed neither inflammatory lesions in lung nor virus antigen-positive cells in the nasal cavity on day 3 p.i. (Fig. 2A and F). After intranasal inoculation with F-ratV, virus antigens were observed immunohistochemically in the respiratory epithelia of the trachea, bronchi, and nasal cavity, which was accompanied by slight inflammatory reactions on day 3 p.i. (Fig. 2B, C, and G). More virus antigen-positive cells were seen in respiratory epithelia including the alveolar area of strain F-ratX-inoculated rats than in Frankfurt 1- or F-ratV-inoculated rats along with severe inflammatory reactions (Fig. 2D, E, and H). Inflammatory reactions, including neutrophils, macrophages, and lymphocytes, as well as microhemorrhage, were seen on day 5 p.i. (Fig. 2D and E). Thus, serial in vivo passage of virus in young rats increased SARS-CoV virulence. None of young F344 rats inoculated with the Frankfurt 1 isolate, F-ratV, or F-ratX showed any obvious clinical signs, and they survived until the observation period.

Increased pathogenicity of serially passaged SARS-CoV in adult rats. In humans, advanced age is associated with greater mortality in SARS patients. Thus, we analyzed potential differences in clinical and pathological features following infection of young (4-week-old females) and adult (7- to 8-month-old males) rats with F-ratX. Since quantities of the F-ratX

TABLE 1. Experimental infection with SARS-CoV in F344 rats

Animal age	Virus strain (100-μl inoculum)	No. of animals with inflammatory reaction/total no. of animals (no. of virus-positive animals/total no. of animals)[a]						No. of neutralization antibody-positive animals/ total no. of animals (titers of antibody to Frankfurt)
		3 days p.i.		7 day p.i.		21 days p.i.		
		Nasal cavity	Lung	Nasal cavity	Lung	Nasal cavity	Lung	
4 wk	Frankfurt	0/3 (1/3)	0/3 (0/3)	0/3 (0/3)	0/3 (0/3)	0/3 (0/3)	0/3 (0/3)	3/3 (2^6, 2^7, 2^7)
4 wk	F-ratX-VeroE6	3/3 (3/3)	3/3 (3/3)	3/3 (3/3)	3/3 (3/3)	0/5 (0/5)	4/5 (0/5)	5/5 (2^7, 2^7, 2^7, 2^8, $<2^8$)
7-8 mo	F-ratX-VeroE6	3/3 (3/3)	3/3 (3/3)	NE	3/3 (2/3)	NE	2/2 (0/2)	2/2[b] (2^7, $<2^8$)

[a] NE, not examined.
[b] Sera were collected on day 14 p.i.

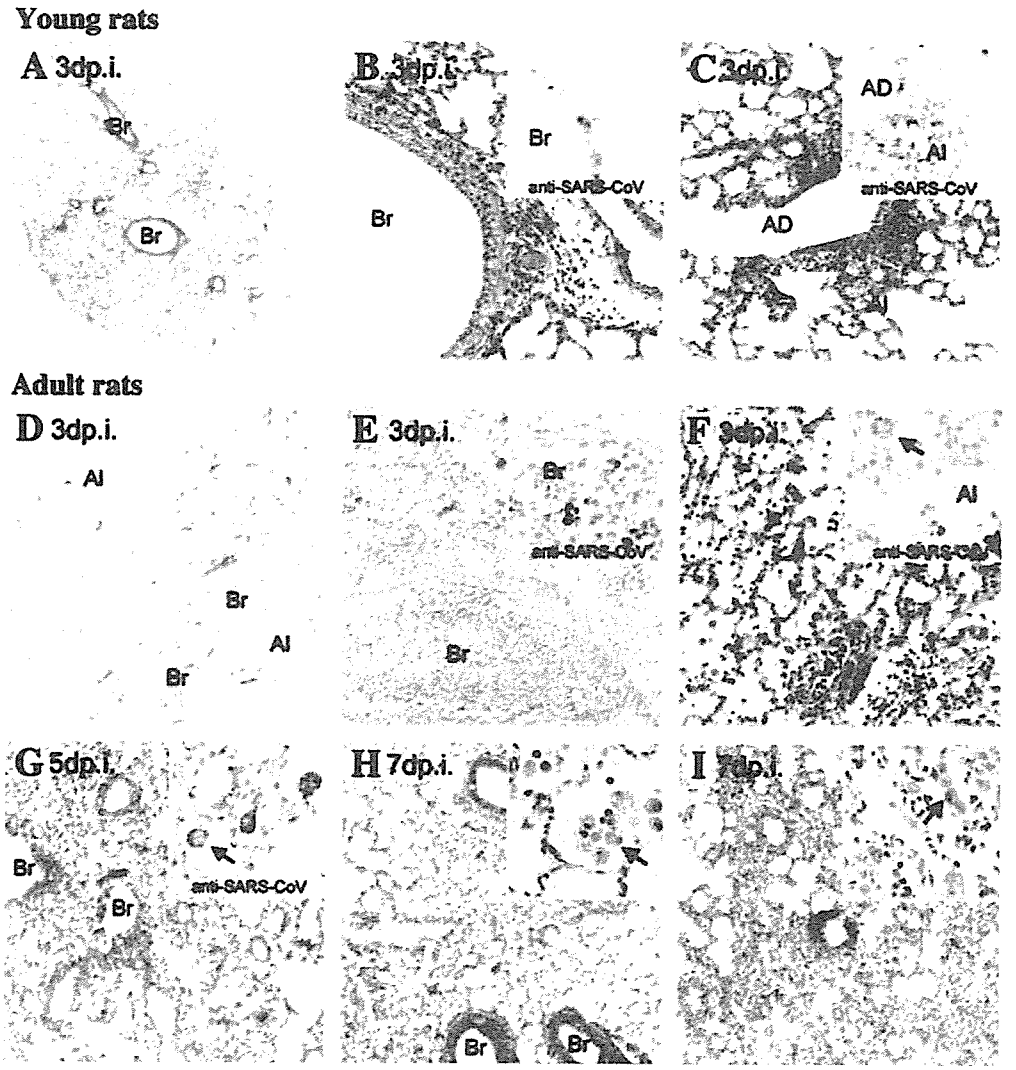

FIG. 3. Histopathological findings in lungs of young and adult F344 rats after intranasal infection with 10-times-serially-passaged SARS-CoV strain F-ratX-VeroE6 on days 3, 5, and 7 p.i. (n = 3). Br, bronchi; Al, alveoli; AD, alveolar duct. (A to C) Inflammatory reactions were observed around the bronchi with leukocytes and lymphocytes (B) and alveolar ducts and alveoli (C) of young F344 rats on day 3 p.i. Immunohistochemical staining with SARS-CoV-specific antibody detected virus antigen-positive cells in those epithelial cells (B and C, insets). (D to F) Massive inflammatory reactions with pulmonary edema and neutrophil and activated macrophage infiltrations were observed in lungs of adult F344 rats on day 3 p.i. Bronchi and alveoli were filled with extensive cellular debris comprised of necrotic epithelia and inflammatory cells (E and F). Immunohistochemical staining by SARS-CoV-specific antibody detected virus antigen-positive cells in necrotic cells and alveolar macrophages (arrow) (E and F, insets). (G) SARS-CoV antigen-positive cells in the alveolar macrophages of adult F344 rats on day 5 p.i. (H and I) Various stages of the inflammatory response and regeneration reaction in the alveoli of adult F344 rats on day 7 p.i. Necrotic macrophages (H, arrow) and effusion substances in alveoli (H, inset) are shown. Mononuclear cell infiltrations and regenerated type II alveolar cells (I, arrow) in alveoli (I, inset) are shown. Magnifications, ×5 (A and D), ×25 (E and G to I), ×50 (B, C, and F), and ×100 (E to I, insets).

preparation were limited, the virus was propagated once in Vero E6 cells (referred to as F-rat-X-VeroE6) before inoculation.

Histopathological features of the lung tissue 3 days after infection with the F-ratX-VeroE6 strain (100 μl of $10^{6.4}$ $TCID_{50}$) differed between young and adult rats (Fig. 3 and Table 1). In young rats without clinical symptoms, inflammatory infiltrates were seen around bronchi, bronchioles, and alveoli (Fig. 3A to C). Virus antigen-positive cells were located at epithelia of the bronchi, bronchioles, and alveoli at day 3 p.i. (Fig. 3B and C, inset). Inflammatory cells such as neutrophils, macrophages, and lymphocytes infiltrated around the affected respiratory tracts (Fig. 3B and C). Mild edema was seen around blood vessels (Fig. 3B). By contrast, after infection, adult rats became lethargic and showed ruffled fur and abdominal breathing. Grossly, a few lobes of the lungs showed congestion, edema, and consolidation at days 3 and 5 p.i. Furthermore, the inflammatory reaction, especially pulmonary edema, was more severe in adult than in young rats (Fig. 3D). Histopathological features of lung tissue on days 3 (Fig. 3E and F), 5 (Fig. 3G), and 7 (Fig. 3H and I) p.i. showed bronchiolitis obliterans organizing pneumonia and diffuse alveolar damage, which are observed in early phases of human SARS. The major inflammatory cells in alveoli were neutrophils and activated

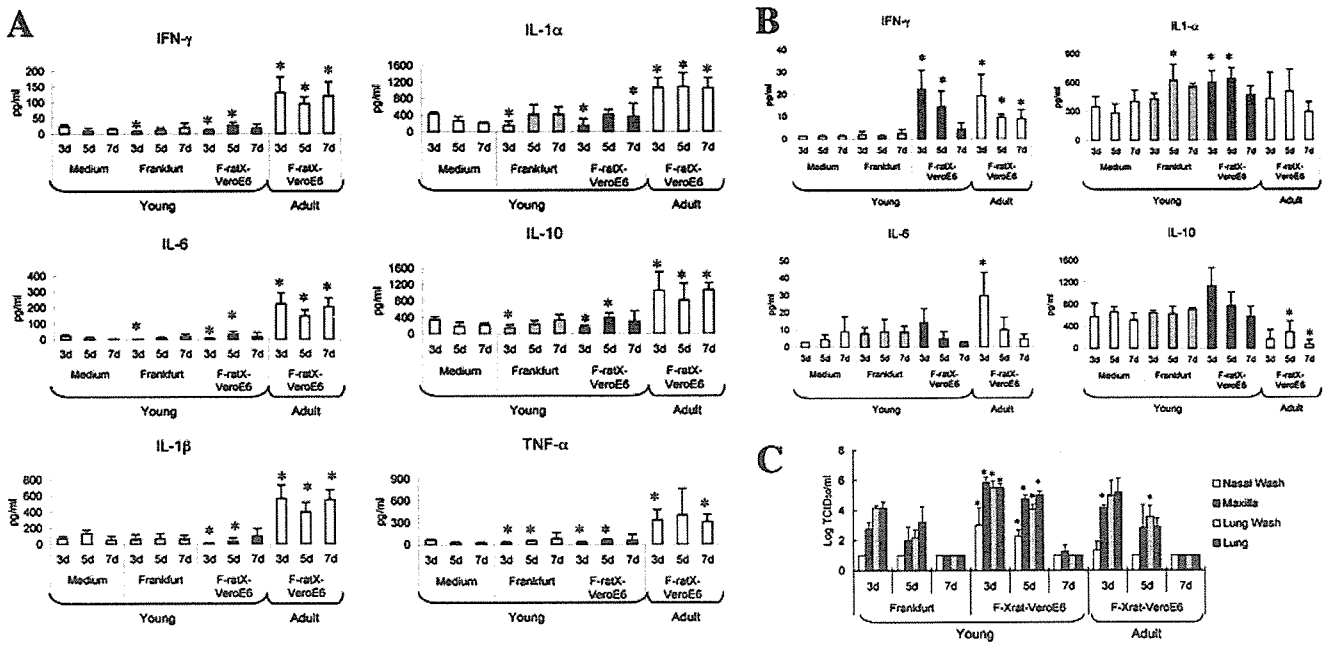

FIG. 4. Induction of inflammatory cytokines at the protein level in sera and lungs following SARS-CoV infection. (A) Cytokine levels in sera of F344 rats after infection. In F-ratX-VeroE6-inoculated adult rats ($n = 5$), serum levels of all cytokines were significantly higher than those seen in young rats ($n = 6$). Cytokine levels of adult F344 rats before infection ($n = 8$) were as follows: IFN-γ, 20.95 pg/ml; TNF-α, 183.77 pg/ml; IL-1α, 371.71 pg/ml; IL-1β, 33.64 pg/ml; IL-6, 22.54 pg/ml; IL-10, 47.07 pg/ml. (B) Cytokine levels in lung homogenates of young and adult F344 rats ($n = 3$) after infection. IFN-γ levels in F-ratX-VeroE6-inoculated young and adult rats were significantly higher than those seen in rats inoculated with the Frankfurt 1 isolate. IL-6 and IL-10 levels of F-ratX-VeroE6-inoculated adult rats were significantly higher and lower, respectively, than those seen in young rats. $*P < 0.05$ compared with medium-inoculated young F344 rats. (C) Virus titers of nasal and lung wash fluids and homogenates of maxilla including nasal cavity and lung of rats ($n = 3$) after infection. The detection limit was $10^{1.5}$ $TCID_{50}$/g of tissue.

macrophages. Fibrin deposition and hyaline membrane formation in alveolar ducts and alveoli were observed (Fig. 3F). By immunohistochemical staining, virus antigen-positive cells were alveolar macrophages and necrotic cells in the lesion (Fig. 3E to G, inset). There were no histopathological changes in the extrapulmonary tissues (brain, spinal cord, heart, liver, kidney, spleen, thymus, and gastrointestinal tract) of any of the animals examined. All the animals survived until the observation period.

Induction of cytokines in SARS-CoV-infected young and adult rats. To analyze the differences in pathogenicity seen in young and adult rats after infection with F-ratX-VeroE6, we examined cytokine levels in sera and lung homogenates (Fig. 4). Young F344 rats inoculated with medium containing 2% fetal bovine serum (100 μl) or the Frankfurt 1 isolate (100 μl of 10^7 $TCID_{50}$) served as controls. F-ratX-VeroE6 strain-infected adult rats showed significantly elevated levels of all 10 cytokines examined ($P < 0.05$) compared with mock-infected young rats (Fig. 4A). Levels of all 10 cytokines were also significantly different ($P < 0.05$) between young and adult rats infected with F-ratX-VeroE6. Adult rats showed elevated levels of IFN-γ ($P < 0.01$), IL-1α ($P = 0.01$), IL-6 ($P < 0.01$), IL-10 ($P < 0.01$), IL-12 ($P < 0.01$), granulocyte-macrophage colony-stimulating factor ($P = 0.02$), IL-4 ($P < 0.01$), and IL-1β ($P < 0.01$) after inoculation (P value between preinfected adult rats and F-ratX-VeroE6-infected adult rats on day 3 p.i.).

In lung homogenates, F-ratX-VeroE6-infected young and adult rats showed elevated levels of IFN-γ ($P = 0.012$ on day 3 and $P = 0.029$ on day 5 for young rats; $P = 0.031$ on day 3, $P < 0.01$ on day 5, and $P = 0.032$ on day 7 for adult rats) compared with mock-infected young rats (Fig. 4B). Elevated levels of IL-6 were observed early in infection in adult rats infected with F-ratX-VeroE6 compared with mock-infected rats ($P = 0.028$). Interestingly, IL-10 levels, which were significantly elevated in sera, deceased significantly in lung homogenates from adult rats infected with F-ratX-VeroE6 ($P = 0.046$ on day 5 and $P < 0.01$ on day 7 between mock-infected young rats; $P < 0.01$ on day 3, $P = 0.055$ on day 5, and $P = 0.009$ on day 7 between strain F-ratX-VeroE6-infected young rats).

Virus titers increased significantly ($P < 0.05$) in nasal and lung washes and in maxillar and lung homogenates of strain F-ratX-VeroE6-infected young rats on days 3 and 5 p.i. compared with strain Frankfurt 1-infected young rats (Fig. 4C). In contrast, in adult rats infected with the F-ratX-VeroE6 strain, virus titers increased significantly ($P < 0.05$) only in maxilla on day 3 p.i. and in lung washes on day 5 p.i. At day 7 p.i., the virus could not be isolated from the lungs of young and adult rats.

Introduction of a missense mutation within the ACE2 binding domain of the S protein of SARS-CoV during serial in vivo passage in rats. Immunohistochemical analyses revealed that ACE2 antigen-positive cells were found in respiratory epithelia of the trachea, bronchi, bronchioles, and alveolar cells of F344 rats (Fig. 5A). The ACE2 protein was most abundantly expressed on cilia of the trachea and intrapulmonary bronchus (Fig. 5A). ACE2 expression was also seen on the apical surface of bronchiolar cells and alveolar pneumocytes. During serial in vivo passage of SARS-CoV in F344 rats, virus replication sites

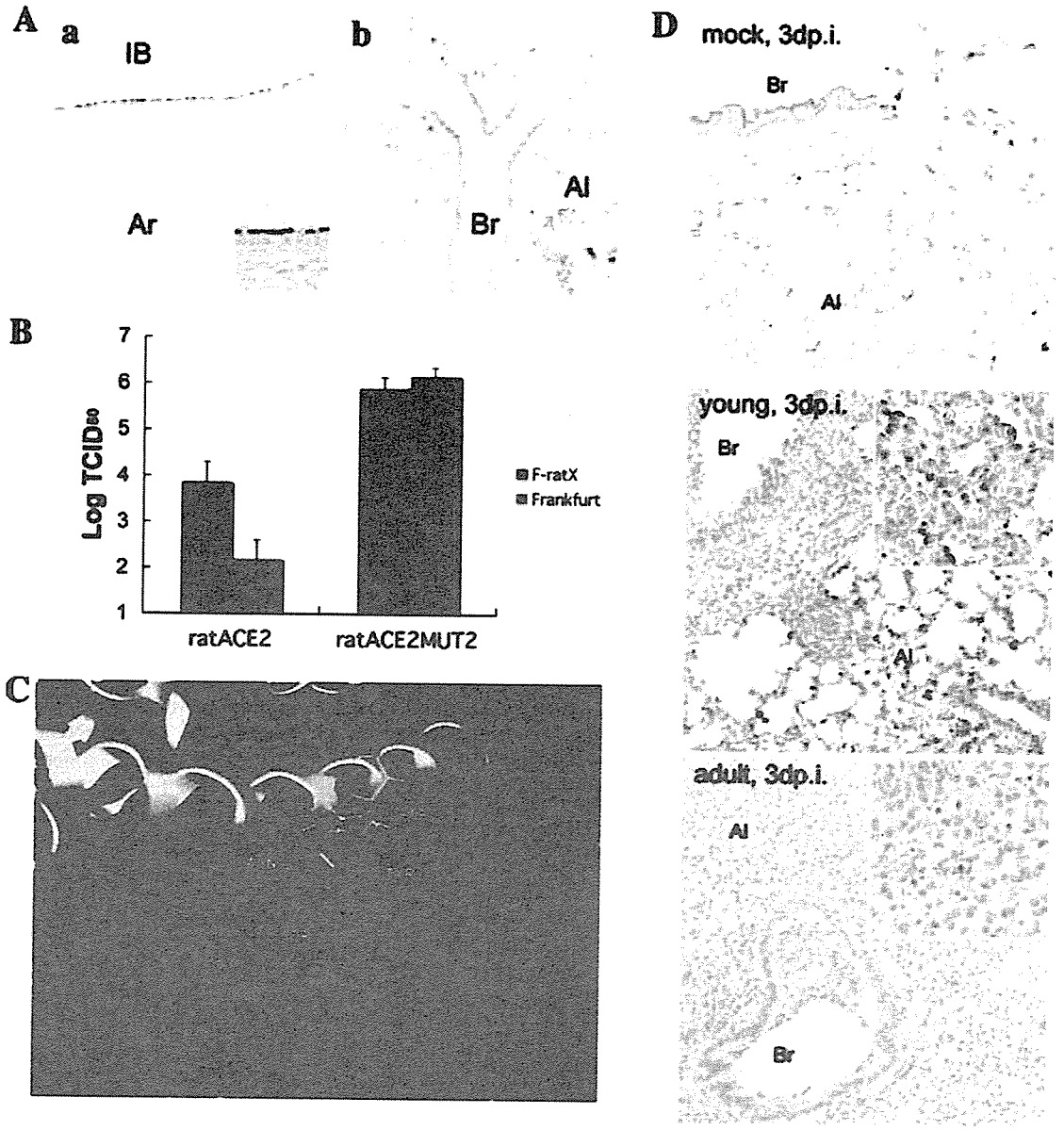

FIG. 5. Correlation of ACE2 expression and infection of serially passaged SARS-CoV in F344 rats. (A) ACE2 antigen-positive cells were detected on respiratory epithelia of the intrapulmonary bronchus (IB), bronchi (Br), and alveolar cells (Al) using immunohistochemical staining with anti-human ACE2 polyclonal antibody (magnification, ×50; inset magnification, ×100). (B) Binding of rat ACE2 to SARS-CoV in ACE2-expressing CHO cells. The F-ratX strain was detected at a higher titer than the Frankfurt 1 isolate in rat ACE2-expressing CHO cells (ratACE2) at 72 h p.i. Both Frankfurt 1 and F-ratX strains replicated in cells expressing variant forms of rat ACE2 in which residues 82 to 84 (NYS) were altered to human ACE2 (MYP) (ratACE2MUT2). The figure represents three experiments with similar results. (C) Molecular modeling of the rat-passaged SARS-CoV spike receptor binding domain complexed with rat ACE2. Green, rat ACE2; blue, Frankfurt 1 isolate; red, F-ratX strain. (D) Localization of ACE2 antigen-positive cells after infection with SARS-CoV on day 3 p.i. by staining with anti-human ACE2 polyclonal antibody. Br, bronchi; Al, alveoli. ACE2 antigen localized to alveolar cells and bronchial epithelial cells in lung of adult rats after mock infection (top, adult F344 rat after intranasal inoculation with MEM). ACE2 antigen-positive cells disappeared in affected bronchi of both young and adult rats (middle, young rat; bottom, adult F344 rat [both after intranasal inoculation with F-ratX-VeroE6]). High expression of ACE2 was found in the apical side of regenerated type II alveolar cells in lesion areas of young rats. Reduced ACE2 expression was observed in inflammatory areas of adult rats (magnification, ×50; inset magnification, ×100).

in lung extended from the bronchus to the alveolar area where ACE2-positive cells were located (Fig. 2 and 5A). ACE2 expression appeared to correlate with the extent and location of virus antigen-positive cells. To examine whether infection by rat-passaged virus is efficiently mediated by rat ACE2, F-ratX and the Frankfurt 1 isolate were inoculated onto rat ACE2-expressing CHO cells. F-ratX replicated more efficiently in these cells than the Frankfurt 1 isolate, while both viruses replicated at the same level in CHO cells expressing an ACE2 variant in which amino acid residues 82 to 84 (NYS) were replaced by the corresponding MYP motif seen in human ACE2 (Fig. 5B). Sequence analysis of the F-ratX strain re-

vealed an A-to-C point mutation at nucleotide 1325 in the region encoding the ACE2 binding site of S1. This mutation resulted in a Y-to-S amino acid change at position 442 in the S protein. The 3-D structure of a complex of the receptor binding domain of the S protein and rat ACE2 predicts that the binding interface might be altered by such a mutation (Fig. 5C). ACE2 expression was examined by immunohistochemistry in young or adult rats after infection with F-ratX-VeroE6 (Fig. 5D). ACE2 antigen-positive cells disappeared in the affected bronchi of both young and adult rats. In young rats, however, ACE2 expression was seen in regenerated type II alveolar cells. By contrast, ACE2 antigen-positive cells were rarely observed in lung lesion areas of adult rats. Thus, ACE2 expression is highly downregulated in the F-ratX-VeroE6-infected adult rats.

DISCUSSION

Our goal was to understand the pathogenesis of SARS-CoV and develop an animal model of SARS. We demonstrated that serial in vivo passage of a human isolate of SARS-CoV, Frankfurt 1, in young F344 rats resulted in the increased virulence of SARS-CoV. The increased infectivity of SARS-CoV after serial passage in F344 rats was correlated with a single amino acid change in the receptor binding domain of the S1 protein, which mediates efficient SARS-CoV binding to ACE2 receptor-expressed rat cells based on both in vitro and structural studies. Adult F344 rats showed severe pathological changes compared with young F344 rats, and those changes were similar to features of human pathology recognized in the SARS epidemic of 2003 to 2004. Here, we demonstrate that both virus and host factors are crucial for the pathogenesis of SARS in vivo.

It has been reported that a virus variant in which 45 nucleotides (nucleotides 27670 to 27714) are deleted within ORF7b emerged upon replication of the Frankfurt 1 isolate in cell culture (37). Thus, for this study, we used a mixture of the original virus and the variant carrying the deletion. The observation that a variant with the deletion was detected in Frankfurt 1-infected rat specimens but was not detected following serial in vivo passaging suggests that the ORF7b may function in viral replication in vivo.

In addition, a Y-to-S amino acid change at residue 442 of the ACE2 binding domain of the S protein occurred during serial passage of the virus in F344 rats. As we have not yet completely sequenced all of the virus genome, it is still possible that another change enhanced virus replication in the rat. However, Li et al. previously demonstrated that residues 479N and 487T within the S-protein receptor binding domain are critical for efficient interaction with human ACE2 and that these residues might be introduced into the virus by mutations during the adaptation of palm civet SARS-CoV, which has 479K and 487S, to humans (20). It seems likely that the Y-to-S mutation at S-protein residue 442 is critical for efficient infection with rat ACE2, since F-ratX replicated more efficiently than the Frankfurt 1 isolate in rat ACE2-expressing CHO cells. Moreover, the 3-D structural prediction of a complex of the S-protein receptor binding domain and rat ACE2 suggests that the binding interface is altered by the Y-to-S mutation. Increased interactions may also be responsible for efficient replication of the virus in rat, since during serial in vivo passage of the virus, replication sites in the lung extended from the bronchus, where ACE2 is most abundantly expressed, to the alveolar area, where it is expressed at a much lower level. Thus, the Y-to-S mutation at residue 442 may partly mediate the increased virulence seen in rats.

Based on immunohistochemical analysis of ACE2 expression in the lung of F344 rats, the ACE2 protein is most abundantly expressed on the cilia of trachea and intrapulmonary bronchi. ACE2 expression appears to correlate with the extent of virus replication sites. Upon infection with F-ratX-VeroE6, ACE2 antigen-positive cells disappeared in the affected bronchi of both young and adult rats. However, ACE2 was expressed in regenerated type II alveolar cells of young rats, but that expression was significantly reduced in adult rats. The downregulation of ACE2 expression by SARS-CoV infection and the presence of the SARS-CoV spike protein in vivo and in vitro have been previously reported (13). Since ACE2 negatively regulates the rennin-angiotensin system by inactivating angiotensin II, which is generated from angiotensin I by ACE, downregulation of ACE2 expression likely blocks the renninangiotensin pathway, which has a crucial role in severe acute lung injury (8, 13). Thus, the downregulation of ACE2 in the lungs of adult rats likely contributes to severe lung injury.

In F-ratX-VeroE6-infected young rats, more virus antigen-positive cells were found in the respiratory epithelia, including the alveolar area, with severe inflammatory reactions; however, rats did not show clinical symptoms of illness. On the other hand, adult rats showed clinical illness and severe pathological changes following F-ratX-VeroE6 infection. Such changes paralleled features seen in human pathologies following the SARS epidemic of the winter of 2003 to 2004 and strongly indicate that host as well as viral factors function in the pathogenesis of SARS in rats. Epidemiological studies of the SARS outbreak of 2003 to 2004 showed that advanced age was a risk factor for an adverse outcome from SARS (1, 3, 16, 27, 38). Roberts et al. previously demonstrated the efficiency of SARS-CoV replication in aged BALB/c mice (33). Our study of animals supports the observation that advanced age is a risk factor for the development of SARS.

Histopathological analysis of adult male F344 rats after F-ratX-VeroE6 infection showed severe inflammatory reactions, especially pulmonary edema. Furthermore, morphologically activated macrophages were observed in alveoli on days 3, 5, and 7 p.i. In contrast, after intranasal inoculation of young rats with F-ratX-VeroE6, inflammatory cell infiltrates consisted of leukocytes and lymphocytes on day 3 p.i. Acute lung injury caused by SARS-CoV is likely a complex pathophysiological process involving inflammatory cytokines released from activated macrophages in alveoli, leading to immune systems dysregulation (25). Our results suggest that the overinduction of inflammatory cytokines in sera and lung homogenates underlies the development of severe inflammation in adult rats. In lung homogenates in particular, IL-6 levels were increased significantly in adult rats after intranasal inoculation with F-ratX-VeroE6 on day 3 p.i.; however, IL-10 levels decreased significantly in adult rats on days 5 and 7 p.i. IL-6, an inflammatory cytokine, is produced by leukocytes, monocytes, endothelial cells, fibroblasts, and alveolar epithelial cells. Serum cytokine levels in SARS patients, particularly IL-6, are signif-

icantly elevated (40). In vitro studies suggest that SARS-CoV replication induces high levels of IL-6 compared with other respiratory viruses (26). Our findings indicate that IL-6 may be produced by predominantly infiltrated leukocytes and macrophages in injured lungs and leads to enhanced inflammatory reactions. By contrast, IL-10, an immunosuppressive cytokine of macrophages, Th2 lymphocytes, and B cells, inhibits TNF-α production and neutrophil activation in lipopolysaccharide-induced acute lung injury and leads to decreases in lung tissue injury (9). Therefore, decreased IL-10 levels in the lung may be responsible for the loss of protective mechanisms, enabling the inflammatory response to continue. It was reported that IL-10 levels increase in the convalescent phase in SARS patients (25). It is currently unclear why elevated cytokine levels are observed in adult rats following F-ratX-VeroE6 infection, since virus replication rates are decreased compared to those for infected young rats. However, our in vivo study suggests that excess cytokine activation may play a key role in the clinical and pathological features of SARS.

In conclusion, we developed an animal model of SARS after SARS-CoV was passaged 10 times in F344 rats and then propagated in Vero E6 cells (F-ratX-VeroE6). This study suggests that both virus and host factors underlie the pathogenesis of SARS. Such an in vivo comparative study of immune responses of young and adult rats using the adapted virus could be useful in further understanding the pathogenesis of SARS, and this model described here should be useful to evaluate vaccine candidates and antiviral agents against SARS-CoV infection.

ACKNOWLEDGMENTS

We thank J. Ziebuhr, Institute of Virology and Immunology, University of Würzburg, Würzburg, Germany, for kindly supplying the Frankfurt 1 isolate. We also thank M. Fujino, I. Hatano, and M. Kataoka, Department of Pathology, National Institute of Infectious Diseases, for technical assistance.

This work was partly supported by a Grant-in Aid for Research on Emerging and Re-Emerging Infectious Diseases from the Ministry of Health, Labor, and Welfare, Japan, and a Grant-in-Aid for Scientific Research from the Ministry of Education, Culture, Sports, Science, and Technology, Japan.

REFERENCES

1. **Booth, C. M., L. M. Matukas, G. A. Tomlinson, A. R. Rachlis, D. B. Rose, H. A. Dwosh, S. L. Walmsley, T. Mazzulli, M. Avendano, P. Derkach, I. E. Ephtimios, I. Kitai, B. D. Mederski, S. B. Shadowitz, W. L. Gold, L. A. Hawryluck, E. Rea, J. S. Chenkin, D. W. Cescon, S. M. Poutanen, and A. S. Detsky.** 2003. Clinical features and short-term outcomes of 144 patients with SARS in the greater Toronto area. JAMA **289:**2801–2809.
2. **Bukreyev, A., E. W. Lamirande, U. J. Buchholz, L. N. Vogel, W. R. Elkins, M. St. Claire, B. R. Murphy, K. Subbarao, and P. L. Collins.** 2004. Mucosal immunisation of African green monkeys (Cercopithecus aethiops) with an attenuated parainfluenza virus expressing the SARS coronavirus spike protein for the prevention of SARS. Lancet **363:**2122–2127.
3. **Donnelly, C. A., A. C. Ghani, G. M. Leung, A. J. Hedley, C. Fraser, S. Riley, L. J. Abu-Raddad, L. M. Ho, T. Q. Thach, P. Chau, K. P. Chan, T. H. Lam, L. Y. Tse, T. Tsang, S. H. Liu, J. H. Kong, E. M. Lau, N. M. Ferguson, and R. M. Anderson.** 2003. Epidemiological determinants of spread of causal agent of severe acute respiratory syndrome in Hong Kong. Lancet **361:**1761–1766.
4. **Drosten, C., S. Günther, W. Preiser, S. van der Werf, H. R. Brodt, S. Becker, H. Rabenau, M. Panning, L. Kolesnikova, R. A. M. Fouchier, A. Berger, A. M. Burguière, J. Cinatl, M. Eickmann, N. Escriou, K. Grywna, S. Kramme, J. C. Mariuguerra, S. Müller, V. Rickerts, M. Stürmer, S. Vieth, H. D. Klenk, A. D. M. E. Osterhaus, H. Schmitz, and H. W. Doerr.** 2003. Identification of a novel coronavirus in patients with severe acute respiratory syndrome. N. Engl. J. Med. **348:**1967–1976.
5. **Fouchier, R. A. M., T. Kuiken, M. Schutten, G. van Amerongen, G. J. J. van Doornum, B. G. van den Hoogen, M. Peiris, W. Lim, K. Stöhr, and A. D. M. E. Osterhaus.** 2003. Koch's postulates fulfilled for SARS virus. Nature **423:**240.
6. **Gao, W., A. Tamin, A. Soloff, L. D'Aiuto, E. Nwanegbo, P. D. Robbins, W. J. Bellini, S. Barratt-Boyes, and A. Gambotto.** 2003. Effects of a SARS-associated coronavirus vaccine in monkeys. Lancet **362:**1895–1896.
7. **Greenough, T. C., A. Carville, J. Coderre, M. Somasundaran, J. L. Sullivan, K. Luzuriaga, and K. Mansfield.** 2005. Pneumonitis and multi-organ system disease in common marmosets (Callithrix jacchus) infected with the severe acute respiratory syndrome-associated coronavirus. Am. J. Pathol. **167:**455–463.
8. **Imai, Y., K. Kuba, S. Rao, Y. Huan, F. Guo, B. Guan, P. Yang, R. Sarao, T. Wada, H. Leong-Poi, M. A. Crackower, A. Fukamizu, C. C. Hui, L. Hein, S. Uhlig, A. S. Slutsky, C. Jiang, and J. M. Penninger.** 2005. Angiotensin-converting enzyme 2 protects from severe acute lung failure. Nature **436:**112–116.
9. **Inoue, G.** 2000. Effect of interleukin-10 (IL-10) on experimental LPS-induced acute lung injury. J. Infect. Chemother. **6:**51–60.
10. **Jia, H. P., D. C. Look, L. Shi, M. Hickey, L. Pewe, J. Netland, M. Farzan, C. Wohlford-Lenane, S. Perlman, and P. B. McCray, Jr.** 2005. ACE2 receptor expression and severe acute respiratory syndrome coronavirus infection depend on differentiation of human airway epithelia. J. Virol. **79:**14614–14621.
11. **Kinomoto, M., M. Yokoyama, H. Sato, A. Kojima, T. Kurata, K. Ikuta, T. Sata, and K. Tokunaga.** 2005. Amino acid 36 in the human immunodeficiency virus type 1 gp41 ectodomain controls fusogenic activity: implications for the molecular mechanism of virus escape from a fusion inhibitor. J. Virol. **79:**5996–6004.
12. **Ksiazek, T. G., D. Erdman, C. S. Goldsmith, S. R. Zaki, T. Peret, S. Emery, S. Tong, C. Urbani, J. A. Comer, W. Lim, P. E. Rollin, S. F. Dowell, A.-E. Ling, C. D. Humphrey, W.-J. Shieh, J. Guarner, C. D. Paddock, P. Rota, B. Fields, J. DeRisi, J. Y. Yang, N. Cox, J. M. Hughes, J. W. LeDuc, W. J. Bellini, L. J. Anderson, and the SARS Working Group.** 2003. A novel coronavirus associated with severe acute respiratory syndrome. N. Engl. J. Med. **348:**1953–1966.
13. **Kuba, K., Y. Imai, S. Rao, H. Gao, F. Guo, B. Guan, Y. Huan, P. Yang, Y. Zhang, W. Deng, L. Bao, B. Zhang, G. Liu, Z. Wang, M. Chappell, Y. Liu, D. Zheng, A. Leibbrandt, T. Wada, A. S. Slutsky, D. Liu, C. Qin, C. Jiang, and J. M. Penninger.** 2005. A crucial role of angiotensin converting enzyme 2 (ACE2) in SARS coronavirus-induced lung injury. Nat. Med. **11:**875–879.
14. **Kuiken, T., R. A. M. Fouchier, M. Schutten, G. F. Rimmelzwaan, G. van Amerongen, D. van Riel, J. D. Laman, T. de Jong, G. van Doornum, W. Lim, A. E. Ling, P. K. S. Chan, J. S. Tam, M. C. Zambon, R. Gopal, C. Drosten, S. van der Werf, N. Escriou, J. C. Manuguerra, K. Stöhr, J. S. M. Peiris, and A. D. M. E. Osterhaus.** 2003. Newly discovered coronavirus as the primary cause of sever acute respiratory syndrome. Lancet **362:**263–270.
15. **Lai, M. M. C., and K. V. Holmes.** 2001. Coronaviridae: the viruses and their replication, p. 1163–1185. *In* D. M. Knipe and P. M. Howley (ed.), Fields virology, 4th ed. Lippincott Williams & Wilkins, Philadelphia, PA.
16. **Lee, N., D. Hui, A. Wu, P. Chan, P. Cameron, G. M. Joynt, A. Ahuja, M. Y. Yung, B. Sc, C. B. Leung, K. F. To, S. F. Lui, C. C. Szeto, S. Chung, and J. J. Y. Sung.** 2003. A major outbreak of severe acute respiratory syndrome in Hong Kong. N. Engl. J. Med. **348:**1986–1994.
17. **Li, B. J., Q. Tang, D. Cheng, C. Qin, F. Y. Xie, Q. Wei, J. Xu, Y. Liu, B. J. Zheng, M. C. Woodle, N. Zhong, and P. Y. Lu.** 2005. Using siRNA in prophylactic and therapeutic regimens against SARS coronavirus in Rhesus macaque. Nat. Med. **9:**944–951.
18. **Li, F., W. Li, M. Farzan, and S. C. Harrison.** 2005. Structure of SARS coronavirus spike receptor-binding domain complexed with receptor. Science **309:**1864–1868.
19. **Li, W., M. J. Moore, N. Vasilieva, J. Sui, S. K. Wong, M. A. Berne, M. Somasundaran, J. L. Sullivan, K. Luzuriaga, T. C. Greenough, H. Choe, and M. Farzan.** 2003. Angiotensin-converting enzyme 2 is a functional receptor for the SARS coronavirus. Nature **426:**450–454.
20. **Li, W., C. Zhang, J. Sui, J. H. Kuhn, M. J. Moore, S. Luo, S. K. Wong, I. C. Huang, K. Xu, N. Vasilieva, A. Murakami, Y. He, W. A. Marasco, Y. Guan, H. Choe, and M. Farzan.** 2005. Receptor and viral determinants of SARS-coronavirus adaptation to human ACE2. EMBO J. **24:**1634–1643.
21. **Li, W., T. C. Greenough, M. J. Moore, N. Vasilieva, M. Somasundaran, J. L. Sullivan, M. Farzan, and H. Choe.** 2004. Efficient replication of severe acute respiratory syndrome coronavirus in mouse cells is limited by murine angiotensin-converting enzyme 2. J. Virol. **78:**11429–11433.
22. **Liang, L., C. He, M. Lei, S. Li, Y. Hao, H. Zhu, and Q. Duan.** 2005. Pathology of guinea pigs experimentally infected with a novel reovirus and coronavirus isolated from SARS patients. DNA Cell Biol. **24:**485–490.
23. **Martina, B. E., B. L. Haagmans, T. Kuiken, R. A. Fouchier, G. F. Rimmelzwaan, G. Van Amerongen, J. S. Peiris, W. Lim, and A. D. Osterhaus.** 2003. SARS virus infection of cats and ferrets. Nature **425:**915.
24. **McAuliffe, J., L. Vogel, A. Roberts, G. Fahle, S. Fischer, W. Shieh, E. Butler, S. Zaki, M. S. Claire, B. Murphy, and K. Subbarao.** 2004. Replication of SARS coronavirus administered into the respiratory tract of African green, rhesus and cynomolgus monkeys. Virology **330:**8–15.
25. **Nicholls, J. M., L. L. Poon, K. C. Lee, W. F. Ng, S. T. Lai, C. Y. Leung, C. M. Chu, P. K. Hui, K. L. Mak, W. Lim, K. W. Yan, K. H. Chan, N. C. Tsang, Y.**

Guan, K. Y. Yuen, and J. S. Peiris. 2003. Lung pathology of fatal severe acute respiratory syndrome. Lancet **361:**1773–1778.

26. **Okabayashi, T., H. Kariwa, S. Yokota, S. Iki, T. Indoh, N. Yokosawa, I. Takashima, H. Tsutsumi, and N. Fujii.** 2006. Cytokine regulation in SARS coronavirus infection compared to other respiratory virus infections. J. Med. Virol. **78:**417–424.
27. **Peiris, J. S., C. M. Chu, V. C. Cheng, K. S. Chan, I. F. Hung, L. L. Poon, K. I. Law, B. S. Tang, T. Y. Hon, C. S. Chan, K. H. Chan, J. S. Ng, B. J. Zheng, W. L. Ng, R. W. Lai, Y. Guan, K. Y. Yuen, and the HKU/UCH SARS Study Group.** 2003. Clinical progression and viral load in a community outbreak of coronavirus-associated SARS pneumonia: a prospective study. Lancet **361:** 1767–1772.
28. **Peiris, J. S. M., S. T. Lai, L. L. M. Poon, Y. Guan, L. Y. C. Yam, W. Lim, J. Nicholls, W. K. S. Yee, W. W. Yan, M. T. Cheung, V. C. C. Cheng, K. H. Chan, D. N. C. Tsang, R. W. H. Yung, T. K. Ng, K. Y. Yuen, and Members of the SARS Study Group.** 2003. Coronavirus as a possible cause of severe acute respiratory syndrome. Lancet **361:**1319–1325.
29. **Ponder, J. W., and D. A. Case.** 2003. Force fields for protein simulations. Adv. Protein Chem. **66:**27–85.
30. **Qin, C., J. Wang, Q. Wei, M. She, W. A. Marasco, H. Jiang, X. Tu, H. Zhu, L. Ren, H. Gao, L. Guo, L. Huang, R. Yang, Z. Cong, L. Guo, Y. Wang, Y. Liu, Y. Sun, S. Duan, J. Qu, L. Chen, W. Tong, L. Ruan, P. Liu, H. Zhang, J. Zhang, H. Zhang, D. Liu, Q. Liu, T. Hong, and W. He.** 2005. An animal model of SARS produced by infection of Macaca mulatta with SARS coronavirus. J. Pathol. **206:**251–259.
31. **Qin, E., H. Shi, L. Tang, C. Wang, G. Chang, Z. Ding, K. Zhao, J. Wang, Z. Chen, M. Yu, B. Si, J. Liu, D. Wu, X. Cheng, B. Yang, W. Peng, Q. Meng, B. Liu, W. Han, X. Yin, H. Duan, D. Zhan, L. Tian, S. Li, J. Wu, G. Tan, Y. Li, Y. Li, Y. Liu, H. Liu, F. Lv, Y. Zhang, X. Kong, B. Fan, T. Jiang, S. Xu, X. Wang, C. Li, X. Wu, Y. Deng, M. Zhao, and Q. Zhu.** 2005. Immunogenicity and protective efficacy in monkeys of purified inactivated Vero-cell SARS vaccine. Vaccine **24:**1028–1034.
32. **Roberts, A., L. Vogel, J. Guarner, N. Hayes, B. Murphy, S. Zaki, and K. Subbarao.** 2005. Severe acute respiratory syndrome coronavirus infection of golden Syrian hamsters. J. Virol. **79:**503–511.
33. **Roberts, A., C. Paddock, L. Vogel, E. Butler, S. Zaki, and K. Subbarao.** 2005. Aged BALB/c mice as a model for increased severity of severe acute respiratory syndrome in elderly humans. J. Virol. **79:**5833–5838.
34. **Rowe, T., G. Gao, R. J. Hogan, R. G. Crystal, T. G. Voss, R. L. Grant, P. Bell, G. P. Kobinger, N. A. Wivel, and J. M. Wilson.** 2004. Macaque model for severe acute respiratory syndrome. J. Virol. **78:**11401–11404.
35. **Sims, A. C., R. S. Baric, B. Yount, S. E. Burkett, P. L. Collins, and R. J. Pickles.** 2005. Severe acute respiratory syndrome coronavirus infection of human ciliated airway epithelia: role of ciliated cells in viral spread in the conducting airways of the lungs. J. Virol. **79:**15511–15524.
36. **Snijder, E. J., P. J. Bredenbeek, J. C. Dobbe, V. Thiel, J. Ziebuhr, L. L. Poon, Y. Guan, M. Rozanov, W. J. Spaan, and A. E. Gorbalenya.** 2003. Unique and conserved features of genome and proteome of SARS-coronavirus, an early split-off from the coronavirus group 2 lineage. J. Mol. Biol. **331:**991–1004.
37. **Thiel, V., K. A. Ivanov, A. Putics, T. Hertzig, B. Schelle, S. Bayer, B. Weissbrich, E. J. Snijder, H. Rabenau, H. W. Doerr, A. E. Gorbalenya, and J. Ziebuhr.** 2003. Mechanisms and enzymes involved in SARS coronavirus genome expression. J. Gen. Virol. **84:**2305–2315.
38. **Tsui, P. T., M. L. Kwok, H. Yuen, and S. T. Lai.** 2003. Severe acute respiratory syndrome: clinical outcome and prognostic correlates. Emerg. Infect. Dis. **9:**1064–1069.
39. **Weingartl, H. M., J. Copps, M. A. Drebot, P. Marszal, G. Smith, J. Gren, M. Andova, J. Pasick, P. Kitching, and M. Czub.** 2004. Susceptibility of pigs and chickens to SARS coronavirus. Emerg. Infect. Dis. **10:**179–184.
40. **Zhang, Y., J. Li, Y. Zhan, L. Wu, X. Yu, W. Zhang, L. Ye, S. Xu, R. Sun, Y. Wang, and J. Lou.** 2004. Analysis of serum cytokines in patients with severe acute respiratory syndrome. Infect. Immun. **72:**4410–4415.

Journal of Medical Virology 78:1509–1512 (2006)

Evaluation of a Novel Vesicular Stomatitis Virus Pseudotype-Based Assay for Detection of Neutralizing Antibody Responses to SARS-CoV

Shuetsu Fukushi,[1]* Tetsuya Mizutani,[1] Masayuki Saijo,[1] Ichiro Kurane,[1] Fumihiro Taguchi,[2] Masato Tashiro,[2] and Shigeru Morikawa[1]

[1]*Department of Virology I, National Institute of Infectious Diseases, Musashimurayama, Tokyo, Japan*
[2]*Department of Virology III, National Institute of Infectious Diseases, Musashimurayama, Tokyo, Japan*

Severe acute respiratory syndrome (SARS)-coronavirus (SARS-CoV) is the causative agent of SARS. The S protein of SARS-CoV is a major target for neutralizing antibodies (Nabs) in infected patients. We developed a neutralization assay using a recombinant vesicular stomatitis virus (VSV) bearing SARS-CoV-S protein (VSV-SARS-St19). A total of 56 serum samples collected from 22 healthcare workers in the Hanoi French Hospital during the SARS epidemic in 2003 were evaluated and compared to the conventional neutralizing assay using infectious SARS-CoV. The results of the neutralization assay using VSV-SARS-St19 pseudotype showed good correlations with those using infectious SARS-CoV. The newly developed neutralization assay was more sensitive to low antibody titers in serum samples. Thus, the VSV-SARS-St19 is a useful tool for detecting Nabs against SARS-CoV. ***J. Med. Virol. 78:1509–1512, 2006.***

KEY WORDS: SARS coronavirus; VSV; pseudotype; neutralization

INTRODUCTION

Severe acute respiratory syndrome (SARS) is a recently emerging life-threatening respiratory disease that has created international concern because of its novelty, communicability, and rapid spread leading to a worldwide outbreak in 2003 [WHO, 2003]. The development of early, rapid, and reliable diagnostic assay systems is a high priority for early vigilance to prevent the spread of the disease. Identification of SARS-coronavirus (SARS-CoV) as the causative agent of SARS has led to the development of genome-based and serological assays for diagnosis of viral infection [Hong et al., 2004; Hourfar et al., 2004; Saijo et al., 2005]. Detection of virus neutralizing antibody (Nab) is important to assess immune responses in SARS-CoV-infected patients. However, conventional virus neutralization assays require handling of infectious, replication-competent SARS-CoV, which raises a number of important safety concerns. Furthermore, it takes at least 2 days to obtain results, because detectable levels of virus replication are required.

Pseudotyped viruses provide a safe tool for virological studies because of their inability to produce infectious progeny virus [Takada et al., 1997]. A quantitative assay with pseudotyped virus infection could facilitate research on virus entry, cell tropism, and virus neutralization. Entry of SARS-CoV into susceptible cells is mediated by binding of the viral S protein to the receptor molecule, angiotensin I-converting enzyme II (ACE2) [Li et al., 2003]. Recently, we reported that recombinant vesicular stomatitis virus (VSV) in which the *G* gene has been replaced by the green fluorescent protein (*GFP*) gene, could be pseudotyped with S protein of SARS-CoV [Fukushi et al., 2005]. Infection with SARS-CoV-S protein-bearing VSV pseudotype (VSV-SARS-St19) is mediated by S protein in an ACE2-dependent manner [Fukushi et al., 2005]. As the SARS-CoV-S protein is a major target for Nabs [Hofmann et al., 2004], it is expected that Nabs in human serum samples also neutralize VSV-SARS-St19. In the present study, a novel Nab assay using VSV-SARS-St19 was developed and its performance was compared with that of a conventional Nab assay using infectious SARS-CoV.

Grant sponsor: Ministry of Health, Labor, and Welfare of Japan; Grant sponsor: Japan Society for Promotion of Science.

*Correspondence to: Shuetsu Fukushi, Special Pathogens Laboratory, Department of Virology I, National Institute of Infectious Diseases, Gakuen 4-7-1, Musashimurayama, Tokyo 208-0011, Japan. E-mail: fukushi@nih.go.jp

Accepted 25 August 2006
DOI 10.1002/jmv.20732
Published online in Wiley InterScience (www.interscience.wiley.com)

MATERIALS AND METHODS

Serum Samples

Fifty-six serum samples collected from 22 healthcare workers in the Hanoi French Hospital, Ho Chi Min City, during a SARS outbreak from February to April 2003 [Saijo et al., 2005] were used in this study. The sera were used for serological analyses after heat-inactivation at 56°C for 30 min.

SARS-CoV

SARS-CoV (HKU39849) used in the present study was kindly supplied by Dr. J.S. Malik Peiris, Department of Microbiology, University of Hong Kong. The virus was propagated on Vero E6 cells and the infectious titer (plaque forming U/ml) was determined on Vero E6 cells.

VSV-SARS-St19 Pseudotype

Generation of VSV-SARS-St19 was performed as described previously [Fukushi et al., 2005]. Briefly, at 24 hr after transfection of 293T cells with pKS-SARS-St19, an expression plasmid encoding a C-terminal-truncated version of the SARS-CoV-S protein, the cells were infected with VSVΔG* (kindly provided by Dr. M.A. Whitt, GTx, Inc.). After absorption for 1 hr, the inoculum was replaced with culture medium and cultured for 24 hr at 37°C in a CO_2 incubator. The culture supernatants were then collected, filtered through a 0.22-μm-pore size filter, and stored at −80°C until use. The titer (infectious units, IU) of pseudotype viruses, which means the number of GFP-positive cells, was determined by end-point dilution using Vero E6 cells.

Neutralizing Assay

As pseudotype VSVs do not produce infectious progeny virus, pseudotype-based neutralization requires higher amounts of pseudotype virus (3,000 IU) than that of SARS-CoV (100 plaque forming units, PFU) in the conventional neutralization assay. The 3,000 IU of VSV-SARS-St19 was the optimum amount for the pseudotype-based neutralization assay. The serum samples were diluted twofold from 1:80 to 1:5,120 with Dulbecco's Modified Eagle's medium (DMEM), containing 5% fetal bovine serum (FBS) and 3,000 IU of VSV-SARS-St19. The mixture was incubated for 1 hr at 37°C for neutralization. After incubation, the mixture was inoculated onto Vero E6 cells seeded on 96-well plates. The infectivity of VSV-SARS-St19 was determined by counting of the number of GFP-positive cells according to the methods described previously [Fukushi et al., 2005]. The Nab titer was defined as the reciprocal of the highest dilution at which more than 50% inhibition of infectivity was observed. The conventional neutralization assay using infectious SARS-CoV (isolate HKU39849, kindly supplied by Dr. J.S. Malik Peiris) was performed as described by Saijo et al. [2005]. Briefly, the heat-inactivated serum samples were diluted twofold with Eagle's minimum essential medium (MEM) containing 2% FBS from 1:10 to 1:320. Each test sample (60 μl by volume) was then mixed with the same volume of SARS-CoV at an infectious dose of 100 PFU and the mixture was incubated for 1 hr at 37°C for neutralization. After incubation, the mixtures were tested for neutralization by cytopathic effect (CPE) inhibition assay using Vero E6 cells. The cutoff value was set at a serum dilution of 1:20. The Nab titer was defined as a reciprocal of the highest dilution at which no CPE was observed.

RESULTS AND DISCUSSION

Recently, we reported that a rabbit antibody raised against purified, inactivated SARS-CoV neutralized VSV-SARS-St19 infection of Vero E6 cells [Fukushi et al., 2005]. To examine whether the Nabs induced in SARS-CoV-infected patients neutralize VSV-SARS-St19 infection, serum samples collected from healthcare workers in the Hanoi French Hospital during the SARS epidemic in 2003 were used. Although clinical information on these subjects was not available, the sera were shown to be sero-converted by conventional SARS-CoV neutralization assay or SARS-CoV-recombinant NP (rNP)-based ELISA [Saijo et al., 2005]. As some SARS-CoV antibody-negative control human sera showed nonspecific anti-pseudotype activity up to a serum dilution of 1:40 (data not shown), samples were tested at dilutions of 1:80 or more, with this value set as the cutoff. VSV-SARS-St19 was preincubated with serum samples serially diluted from 1:80 to 1:5,120. Then, the preincubated virus was inoculated onto Vero E6 cells and infectious foci were counted. Figure 1 shows dynamic cumulative percentages of pseudotype infectivity using serum samples collected from three subjects (S1, S2, and S3). Samples were considered Nab-positive when VSV-SARS-St19 infection was inhibited by 50% or greater as compared to serum-negative control. There were no Nabs detected in the serum samples collected at earlier stages (i.e., serum samples collected on March 17 from S1 and S3 and serum sample from S2 collected on March 27), as the infectivity of the pseudotype in the presence of diluted serum samples ranged from 70.1 to 101.7% of the serum negative control (data not shown). In contrast, the serum samples collected from these three subjects at later stages (March 29) showed a reduction in the number of foci by more than 50% (Fig. 1). The results indicated that these serum samples contained Nabs to VSV-SARS-St19. The Nab titers were defined as the reciprocal of the highest dilution at which more than 50% inhibition of infectivity was observed. Serum samples collected on March 29 from S1, S2, and S3 were shown to have Nabs with titers of 1,280; 320; and 320, respectively. Nab titers using SARS-CoV on conventional neutralization assay for S1, S2, and S3 were $\geq$640, 80, and 160, respectively (data not shown). The results of neutralization assay using VSV-SARS-St19 were in good agreement with those of neutraliza-

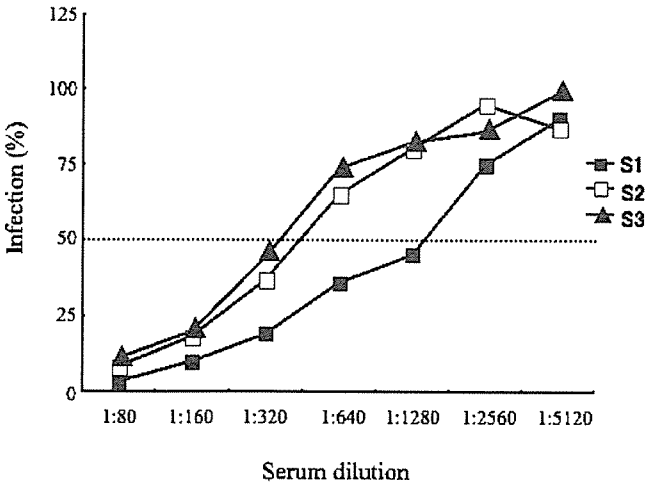

Fig. 1. Neutralization assay using VSV-SARS-St19 pseudotype. A: Inhibition of VSV-SARS-St19 infection by serum samples. Prior to infection of Vero E6 cells, VSV-SARS-St19 pseudotypes were pre-incubated with two serum samples collected from each of three subjects (S1, S2, and S3) at the indicated dilutions. Serum samples were collected at March 17 and 29 for the subjects S1 and S3, whereas serum samples were collected at March 27 and 29 for the subject S2. The infectivity of the pseudotype, determined by counting GFP-positive cells, in the absence of serum was considered 100%. The infectivity of the pseudotype in the presence of diluted serum samples collected at later stages (March 29, 2003) was shown.

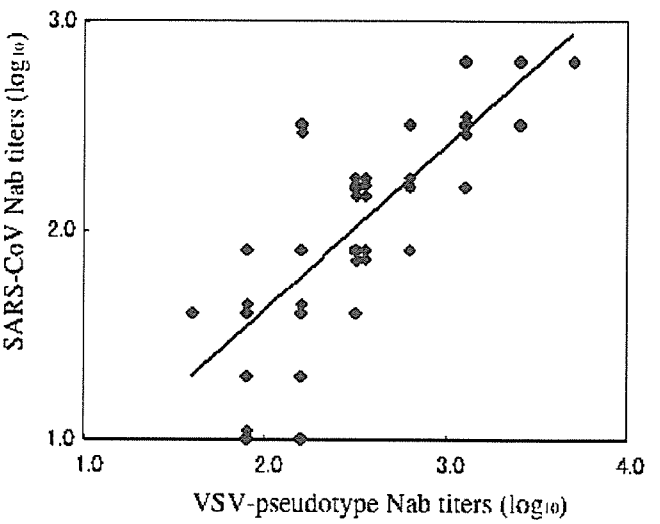

Fig. 2. Correlation between neutralizing antibody titers measured using VSV-SARS-St19 pseudotype and those measured using SARS-CoV. The correlation coefficient was 0.77. Nab titers (log_{10}) values with SARS-CoV neutralization assay plotted between 1 and 3 on the y-axis scale whereas those with VSV-based assay plotted between 1 and 4 on the x-axis scale.

tion assay using SARS-CoV and Nab titers obtained with VSV-based neutralization assay were two- to fourfold higher than those obtained with conventional neutralization assay.

To validate the VSV-SARS-St19-based neutralization assay, an additional neutralization assay was carried out on a subset of 53 serum samples collected from healthcare workers in the Hanoi French Hospital. The titers of Nabs determined using VSV-SARS-St19 were compared with those using a conventional neutralization assay with infectious SARS-CoV. Thirty-three serum samples were shown to be positive by either neutralization assay. As shown in Figure 2, there was a significant positive correlation (correlation coefficient = 0.77) between the Nab titers determined by VSV-SARS-St19 and SARS-CoV. Of the 36 serum samples positive by VSV-SARS-St19 neutralization assay, 3 were negative by the conventional neutralization assay (Table I). The possibility of false-positive results of these three samples in VSV-SARS-St19-based assay cannot be excluded. However, it seems likely that these three sera had extremely low titers of Nabs to SARS-CoV, as sera collected from the same subjects 9 or 14 days later had high Nabs titers (from 320 to 640) to VSV-SARS-St19 (data not shown). Furthermore, among these three serum samples, one was positive by rNP-based ELISA with an OD_{405} value of 0.568 at 1:100 dilution (data not shown), indicating that the serum contained antibodies to SARS-CoV. Taken together, these results suggest that the VSV-SARS-St19-based neutralization assay was more sensitive than the conventional neutralization assay using SARS-CoV. This assumption was supported by the observation that the Nab titers measured using VSV-SARS-St19 were higher than those measured by the conventional neutralization assay (Figs. 1 and 2). Neutralization data obtained with 56 serum samples, with neutralization assay using SARS-CoV as a reference method, showed that the sensitivity and specificity of VSV-SARS-St19-based neutralization assay were 97 and 86%, respectively (Table I). Neutralization assay is the gold standard in testing for antibodies to SARS-CoV because of its specificity and sensitivity. As comparative neutralization data indicated a good correlation with conventional neutralization assay using SARS-CoV, VSV-SARS-St19-based neutralization assay is a reliable serological test for SARS-CoV infection.

The pseudotype-based neutralization assay does not require handling of infectious SARS-CoV. This safety concern has led several laboratories to utilization of replication-incompetent retrovirus-based SARS-CoV-S pseudotype for assessing Nabs to SARS-CoV [Nie et al., 2004; Temperton et al., 2005]. The retrovirus pseudotype-based neutralization assay is shown to be both sensitive and specific for conventional neutralization assay [Nie et al., 2004; Temperton et al., 2005]. However, time required to determine the virus infectivity in the

TABLE I. Comparison of the Results of the Neutralization Assay Using VSV-SARS-St19 Pseudotype With Those Using SARS-CoV

	VSV-SARS-S pseudotype		
SARS-CoV	Positive	Negative	Total
Positive	33	1	34
Negative	3[a]	19	22
Total	36	20	56

[a]One serum sample was positive in the rNP-based ELISA.

retrovirus system is 48 hr, which is similar to the time required for SARS-CoV to replicate to a level that results in plaque-forming or cytopathic effects in infected cells. In contrast, use of the VSVΔG* system has the advantage of rapid detection of pseudotype infection [Ogino et al., 2003]. Recently, we reported that upon infection of Vero E6 cells by VSV-SARS-St19 pseudotype, infected cells can be detected at 7 hr post-infection due to rapid expression of GFP in the VSVΔG* system [Fukushi et al., 2005]. Furthermore, quantitative analysis of VSV-SARS-St19 infection can be performed easily by counting the number of GFP-positive cells using ImageJ software (http://rsb.info.nih.gov/ij/). Thus, this novel Nab assay system allows the measurement of SARS-CoV-specific Nabs within 1 day.

In the present study, we established a rapid and safe SARS-CoV-neutralization assay using VSV-SARS-St19 pseudotype. The results obtained using this system showed a good correlation with those obtained using the conventional neutralization assay with SARS-CoV. Furthermore, the novel Nab assay appeared to be more sensitive to low antibody titers in serum samples. Thus, VSV-SARS-St19 provides a useful tool for detecting Nabs against SARS-CoV.

ACKNOWLEDGMENTS

We thank Dr. J.S. Malik Peiris, Department of Microbiology, University of Hong Kong, for providing SARS-CoV (HKU-39849), Dr. M.A. Whitt, GTx, Inc., for providing VSVΔG*, and Dr. Long H.T. and Dr. Hanh N.T., National Institute of Hygiene and Epidemiology, for providing serum samples collected from healthcare workers in the Hanoi French Hospital. We also thank Ms. M. Ogata for her assistance. This work was supported in part by a grant-in-aid from the Ministry of Health, Labor, and Welfare of Japan and the Japan Society for Promotion of Science.

REFERENCES

Fukushi S, Mizutani T, Saijo M, Matsuyama S, Miyajima N, Taguchi F, Itamura S, Kurane I, Morikawa S. 2005. Vesicular stomatitis virus pseudotyped with severe acute respiratory syndrome coronavirus spike protein. J Gen Virol 86:2269–2274.

Hofmann H, Geier M, Marzi A, Krumbiegel M, Peipp M, Fey GH, Gramberg T, Pohlmann S. 2004. Susceptibility to SARS coronavirus S protein-driven infection correlates with expression of angiotensin converting enzyme 2 and infection can be blocked by soluble receptor. Biochem Biophys Res Commun 319:1216–1221.

Hong TC, Mai QL, Cuong DV, Parida M, Minekawa H, Notomi T, Hasebe F, Morita K. 2004. Development and evaluation of a novel loop-mediated isothermal amplification method for rapid detection of severe acute respiratory syndrome coronavirus. J Clin Microbiol 42:1956–1961.

Hourfar MK, Roth WK, Seifried E, Schmidt M. 2004. Comparison of two real-time quantitative assays for detection of severe acute respiratory syndrome coronavirus. J Clin Microbiol 42: 2094–2100.

Li W, Moore MJ, Vasilieva N, Sui J, Wong SK, Berne MA, Somasundaran M, Sullivan JL, Luzuriaga K, Greenough TC, Choe H, Farzan M. 2003. Angiotensin-converting enzyme 2 is a functional receptor for the SARS coronavirus. Nature 426:450–454.

Nie Y, Wang P, Shi X, Wang G, Chen J, Zheng A, Wang W, Wang Z, Qu X, Luo M, Tan L, Song X, Yin X, Ding M, Deng H. 2004. Highly infectious SARS-CoV pseudotyped virus reveals the cell tropism and its correlation with receptor expression. Biochem Biophys Res Commun 321:994–1000.

Ogino M, Ebihara H, Lee BH, Araki K, Lundkvist A, Kawaoka Y, Yoshimatsu K, Arikawa J. 2003. Use of vesicular stomatitis virus pseudotypes bearing hantaan or seoul virus envelope proteins in a rapid and safe neutralization test. Clin Diagn Lab Immunol 10: 154–160.

Saijo M, Ogino T, Taguchi F, Fukushi S, Mizutani T, Notomi T, Kanda H, Minekawa H, Matsuyama S, Long HT, Hanh NT, Kurane I, Tashiro M, Morikawa S. 2005. Recombinant nucleocapsid protein-based IgG enzyme-linked immunosorbent assay for the serological diagnosis of SARS. J Virol Methods 125:181–186.

Takada A, Robison C, Goto H, Sanchez A, Murti KG, Whitt MA, Kawaoka Y. 1997. A system for functional analysis of Ebola virus glycoprotein. Proc Natl Acad Sci USA 94:14764–14769.

Temperton NJ, Chan PK, Simmons G, Zambon MC, Tedder RS, Takeuchi Y, Weiss RA. 2005. Longitudinally profiling neutralizing antibody response to SARS coronavirus with pseudotypes. Emerg Infect Dis 11:411–416.

WHO. 2003. Summary of probable cases with onset of illness from 1 November 2002 to 31 July 2003. World Health Organization.

Available online at www.sciencedirect.com
SCIENCE DIRECT®
ELSEVIER
Biochemical and Biophysical Research Communications 347 (2006) 261–265
BBRC
www.elsevier.com/locate/ybbrc

Mechanisms of establishment of persistent SARS-CoV-infected cells

Tetsuya Mizutani [a,*], Shuetsu Fukushi [a], Koji Ishii [b], Yuko Sasaki [c], Tsuyoshi Kenri [c], Masayuki Saijo [a], Yumi Kanaji [d], Kinji Shirota [d], Ichiro Kurane [a], Shigeru Morikawa [a]

[a] *Department of Virology 1, National Institute of Infectious Diseases, Gakuen 4-7-1, Musashimurayama, Tokyo 208-0011, Japan*
[b] *Department of Virology 2, National Institute of Infectious Diseases, 1-23-1 Toyama, Shinjuku-ku, Tokyo 162-8640, Japan*
[c] *Department of Bacteriology 2, National Institute of Infectious Diseases, Gakuen 4-7-1, Musashimurayama, Tokyo 208-0011, Japan*
[d] *Research Institute of Biosciences, Azabu University, 1-71-1 Futinobe, Sagamihara-shi, Kanagawa 229- 8501, Japan*

Received 6 June 2006
Available online 22 June 2006

Abstract

Previously, we reported the establishment of cells with persistent SARS-CoV infection after apoptotic events and showed that both JNK and PI3K/Akt signaling pathways are important for persistence by treatment with inhibitors at the early stages of SARS-CoV infection. However, the mechanisms of establishment of persistent infection are still unclear. In this study, we investigated which signaling pathways play important roles in escape from apoptosis in cells infected with SARS-CoV. In persistently infected cells at 50 h.p.i., PI3K/Akt, JNK, p38 MAPK and Bcl-2 were phosphorylated and the protein levels of Bcl-2 and Bcl-xL were increased. When surviving cells were treated with the JNK-specific inhibitor, SP600125, at 50 h.p.i., all cells died, suggesting that the JNK signaling pathway is necessary for maintenance of persistently infected cells. Among the signaling pathways in persistently infected cells, Akt and JNK were phosphorylated in SARS-CoV-nucleocapsid (N) protein-expressing Vero E6 cells using vaccinia viral vector (DIs), strongly suggesting that N protein-induced phosphorylation of Akt and JNK are necessary to establish persistence. These results indicated that at least four proteins, Akt, JNK, Bcl-2 and Bcl-xL, are necessary for survival of persistently SARS-CoV-infected cells.

Keywords: SARS; JNK; Bcl-2; Bcl-xL; Nucleocapsid protein

Severe acute respiratory syndrome (SARS) is a newly discovered infectious disease with atypical pneumonia caused by SARS coronavirus (SARS-CoV). SARS became a global health threat due to its rapid transmission and high fatality rate [1,2].

Vero E6 is a cell line derived from African green monkey kidney cells and is sensitive to SARS-CoV. Many laboratories use this cell line to study SARS-CoV. Infection of Vero E6 cells with SARS-CoV induces apoptosis *via* activation of caspase-3 [3]. Akt and mitogen-activated protein kinases (MAPKs), including c-Jun N-terminal protein kinase (JNK), extracellular signal-related kinase (ERK) 1/2, and p38 MAPK, are phosphorylated in SARS-CoV-infected Vero E6 cells [3–5]. Especially, activation of p38 and inactivation of Akt by SARS-CoV infection induce cytopathic effects and apoptosis in virus-infected cells, respectively. Phosphorylation of p38 MAPK is known to regulate signal transducer and activator of transcription 3 and 90 kDa ribosomal S6 kinases [5,6]. Although the majority of virus-infected cells die by apoptosis, we found that a small population of virus-infected cells remained alive and these cells grew with production of virus [7]. Four groups, including ours, independently reported persistent infection of cultured cells by SARS-CoV [8–10]. We found that JNK and PI3K/Akt signaling pathways are important for the establishment of persistent SARS-CoV infection in Vero E6 cells when these specific inhibitors were added soon after viral adsorption.

In this study, we further analyzed the mechanisms of establishment of persistent SARS-CoV infection in Vero

* Corresponding author. Fax: +81 42 564 4881.
E-mail address: tmizutan@nih.go.jp (T. Mizutani).

0006-291X/$ - see front matter © 2006 Elsevier Inc. All rights reserved.
doi:10.1016/j.bbrc.2006.06.086

E6 cells. We found that anti-apoptotic proteins, Bcl-2 and Bcl-xL, are important for persistent infection. Nucleocapsid (N) protein of SARS-CoV was suggested to play important roles in phosphorylation of Akt and JNK.

Materials and methods

Cells and virus. Vero E6 cells were subcultured routinely in 75-cm^3 flasks in Dulbecco's modified Eagle's medium (DMEM; Sigma, St. Louis, MO, USA) supplemented with 0.2 mM L-glutamine, 100 U/ml penicillin, 100 μg/ml streptomycin, and 5% (v/v) fetal bovine serum (FBS), and maintained at 37 °C in an atmosphere of 5% CO_2. The medium was changed to 2% FBS DMEM before virus infection. SARS-CoV, which was isolated as Frankfurt 1 and kindly provided by Dr. J. Ziebuhr, was used in the present study. Infection was usually performed at a multiplicity of infection (m.o.i.) of 5. DIs-N expressing N RNA of SARS-CoV and DIs-GFP expressing GFP RNA were described in our previous study [11]. Confluent Vero E6 cells were infected with DIs-N and -GFP at 5 m.o.i.

Fixing and staining of cells. The cells in 24-well plates were fixed with 10% formaldehyde for at least 24 h, and stained with 0.1% naphthol blue-black for 30 min. This convenient method was described by Everitt and Wohlfart for determination of the actual or relative number of cells in anchorage culture [12]. After washing out with water, the plates were scanned with a GT-9400UF scanner (Epson, Tokyo, Japan). The dye–protein complexes were released hydrolytically with 0.1 M NaOH and measured spectrophotometrically at 660 nm. When cells and the supernatant contained infectious SARS-CoV, the cell number was counted using this method. The number of cells that did not contain SARS-CoV was counted using the WST-1 cell proliferation assay system (Takara, Shiga, Japan).

Inhibitors. The JNK inhibitor, SP600125, and PI3K/Akt inhibitor, LY294002, were purchased from Calbiochem (San Diego, CA, USA) and Cell Signaling Technology Inc. (Beverly, MA, USA), respectively. These inhibitors were dissolved in dimethyl sulfoxide (DMSO) at a concentration of 10 mM. The same volume of DMSO alone was used as a control.

Western blotting. The whole-cell extracts were electrophoresed on 5–20% gradient polyacrylamide gels, and transferred electrophoretically onto PVDF membranes (Immobilon-P; Millipore, Bedford, MA, USA). In the present study, we applied two sets of samples to polyacrylamide gels, and the membranes were divided into two halves after blotting, or membranes were examined once using a LumiGLO Elite chemiluminescent system (Kirkegaard and Perry Laboratories, Gaithersburg, ML, USA), and then stripped using Restore Western blot stripping buffer (Pierce, Rockford, IL, USA) for the second detection. The following antibodies, obtained from Cell Signaling Technology Inc., were used in the present study at a dilution of 1:1000: rabbit anti-phospho Akt (Ser473) antibody, rabbit anti-Akt antibody, rabbit anti-phospho ERK (Thr202/Tyr204) antibody, rabbit anti-ERK antibody, rabbit anti-p38 MAPK (Thr180/Tyr182) antibody, rabbit anti-p38 MAPK antibody, rabbit anti-phospho SAPK/JNK (Thr183/Tyr185) antibody, rabbit anti-SAPK/JNK antibody, rabbit anti-phospho Bcl-2 (Ser 70) antibody, and anti-Bcl-xL antibody. Mouse anti-Bcl-2 antibody was purchased from BD Biosciences (Franklin Lakes, NJ, USA) and used at a dilution of 1:500. Mouse anti-β-actin antibody was purchased from Sigma and used at a dilution of 1:5000. Rabbit anti-SARS Nucleocapsid protein antibody was described previously [3].

Results

Phosphorylation of signaling pathways in cells persistently infected by SARS-CoV

As indicated in our previous studies, apoptotic signals, cleaved caspase-3 and DNA fragmentation, are detected at 18 and 24 h post-infection (h.p.i.) in SARS-CoV-infected Vero E6 cells [3]. At 24 h.p.i., cells begin to show rounding and persistently infected cells are observed after 48 h.p.i. To investigate which signaling pathways are phosphorylated in persistently SARS-CoV-infected cells, protein samples were obtained from these cells at 50 h.p.i. Vero E6 cells were prepared at confluency in T-25 flasks with 2% fetal bovine serum (FBS) containing Dulbecco's modified Eagle's medium (DMEM), and infected with SARS-CoV at 5 m.o.i. On the other hand, Vero E6 cells were prepared in T-25 flasks at several concentrations with 2% FBS containing DMEM as controls because surviving cell number is different (less than 5% of total cells) in each experiment. At 50 h.p.i., surviving cells and controls were washed with 2% FBS containing DMEM 5 times (with pipetting 25 times). Although most dead cells were washed out, a fraction of dead cells were attached to surviving cells and could not be removed completely by washing. As phosphorylation status of signaling pathways sometimes changes following trypsinization and centrifugation, sample buffer for Western blotting analysis was added directly to the washed cells. We obtained a protein sample from mock-infected cells, with a similar cell number to persistently infected cells. The protein samples seemed to contain a maximum of 50% proteins from surviving cells. Western blotting analysis was performed using antibodies to phosphorylated proteins of signaling pathways. As shown in Fig. 1, Akt, JNK, and p38 MAPK were phosphorylated in surviving cells. On the other hand, Akt was phosphorylated in control cells, while JNK and p38 MAPK were not. As Akt was dephosphorylated in both confluent and subconfluent cells after 18 h.p.i. as shown in our previous studies [4,13], detection of strongly phosphorylated Akt was

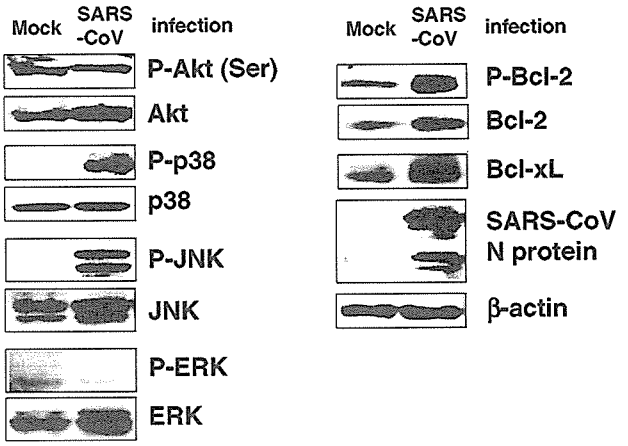

Fig. 1. Phosphorylation status of signaling pathways in persistently SARS-CoV-infected cells. Vero E6 cells were prepared at confluency in T-25 flasks with 2% fetal bovine serum (FBS) containing Dulbecco's modified Eagle's medium (DMEM), and infected with SARS-CoV at 5 m.o.i. At 50 h.p.i., surviving cells and controls were washed 5 times with 2% FCS containing DMEM (pipetting a total of 25 times). Mock-infected subconfluent cells, similar in number to surviving cells that had escaped from apoptosis by SARS-CoV infection, were also washed in the same manner. Western blotting analysis was performed using these protein samples.

suggested to reflect a feature of surviving cells that had escaped from cell death. In addition, the phosphorylated Akt in surviving cells indicated anti-apoptotic activity. The levels of the anti-apoptotic proteins, Bcl-2 and Bcl-xL, and phosphorylated Bcl-2, were also increased in surviving cells. The anti-apoptotic Bcl-2 family proteins, Bcl-2 and Bcl-xL, play important roles in inhibiting mitochondria-dependent cell death pathways [14]. This result suggested that Akt and JNK are important to establish persistent infection as indicated in our previous study, and that Bcl-xL and Bcl-2 are important for survival. Interestingly, p38 MAPK was strongly phosphorylated in surviving cells, suggesting that persistently infected cells consist of a balance between cell death and survival.

Importance of PI3K/Akt and JNK for establishment of persistently virus-infected cells

In our previous study, we showed that treatment of Vero E6 cells with the JNK inhibitor, SP600125, and PI3K/Akt inhibitor, LY294002, 1 h after inoculation with SARS-CoV prevented persistent SARS-CoV infection [7]. Therefore, we concluded that activation of JNK and PI3K/Akt by SARS-CoV infection is important for the establishment of persistence. To investigate whether these inhibitors affect the establishment of viral persistence in cells at the late stage of SARS-CoV infection, cells were treated with inhibitors at 50 h.p.i. As shown in Fig. 2A and B, SP600125 killed the cells completely, while LY294002 did not. As LY294002 has an inhibitory effect on cell proliferation, as indicated in Fig. 2C and in our previous study [13], the growth rate of persistently infected cells was slow. On the other hand, treatment with SP600125 in the absence of SARS-CoV infection did not affect cell proliferation. As Akt in virus-infected cells was dephosphorylated after 18 h.p.i., as shown in our previous studies [4,13], phosphorylation of Akt at the early stage of infection may be important for preventing apoptosis. However, this result strongly suggested that once persistence is established, phosphorylation of Akt is not necessary for survival. Therefore, we concluded that activation of PI3K/Akt is essential for the establishment of persistent infection with SARS-CoV at time points before cell death, whereas activation of JNK is required at the time of establishment of persistence.

Phosphorylation of signaling pathways by SARS-CoV-nucleocapsid protein

Next, we investigated which signaling pathways are phosphorylated by nucleocapsid (N) protein of SARS-CoV because several reports indicated that expression of N protein induces phosphorylation of signaling pathways. Surjit et al. reported that ERK, phosphorylated Akt and Bcl-2 are down-regulated, whereas JNK, p38 MAPK activation, activated caspase-3 and -7 are up-regulated in COS-1 cells in the absence of growth factors [15]. They

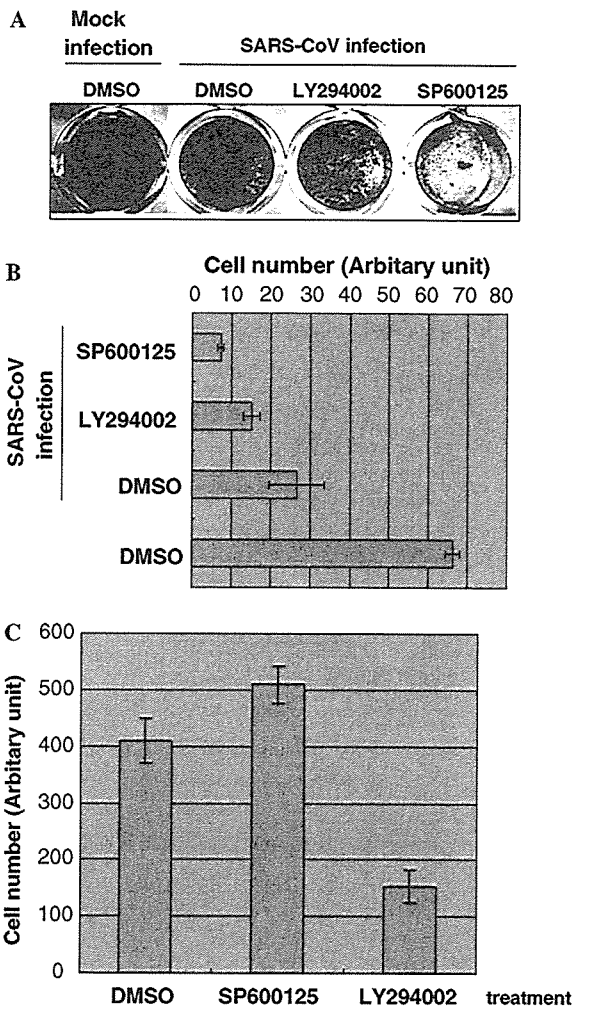

Fig. 2. Effects of JNK and PI3K/Akt inhibitors on cell viability of persistently SARS-CoV-infected cells. (A) Confluent Vero E6 cells in 24-well plates were infected with SARS-CoV for 50 h, and then LY294002 (10 μM) and SP600125 (20 μM) were added to the cells. All wells contained the same volume of DMSO. After incubation for 7 days, the cells were fixed with 10% formaldehyde and stained with 0.1% naphthol blue-black. (B) Stained cells were quantified by measuring the absorbance at OD_{660} with addition of NaOH. (C) Subconfluent cells were treated with inhibitors for 5 days, and then cells were counted using the WST-1 cell proliferation assay system [6].

suggested that N protein is able to induce apoptosis under stress conditions. To understand which signaling pathways are phosphorylated by N protein in Vero E6 cells persistently infected with SARS-CoV, we made an N expression plasmid. Transfection of the N expression plasmid was performed using transfection reagents, Magnetfection and VeroFect (OZ Biosciences, Marseille, France), which our screen of transfection reagents suggested to be the best transfection systems for Vero E6 cells, which have low transfection efficiency (data not shown). However, levels of expression of N protein by these two reagents were far lower than those in SARS-CoV-infected Vero E6 cells. Therefore, we next used the vaccinia virus expression system (DIs-N) [11]. Vero E6 cells were infected with DIs-N at 5 m.o.i. and protein samples were obtained at 18 h.p.i.

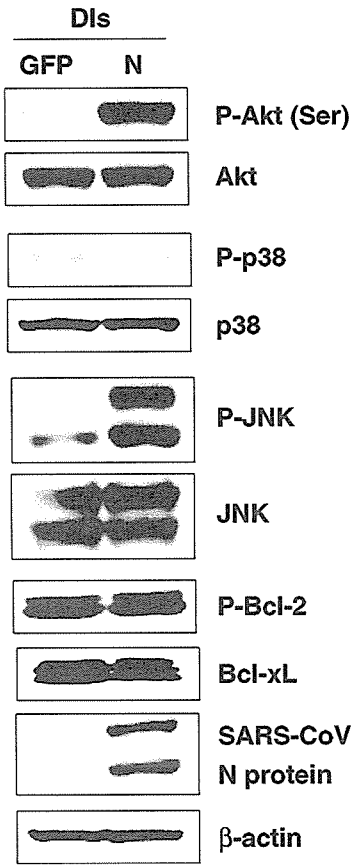

Fig. 3. Modulation of signaling pathways by N expression. Confluent Vero E6 cells in 24-well plates were infected with DIs-N and DIs-GFP at 5 m.o.i. Protein samples were obtained at 18 h.p.i. and Western blotting analysis was performed.

We used DIs-GFP, which expresses GFP protein in infected cells, as a control at the same m.o.i. As shown in Fig. 3, both Akt and JNK were phosphorylated in DIs-N-infected cells as compared with DIs-GFP-infected cells. There was no significant difference in the amount of Bcl-2, Bcl-xL, and phosphorylated p38 MAPK. This result suggested that phosphorylation of Akt and JNK induced by N protein in SARS-CoV-infected Vero E6 cells plays important roles for the establishment of persistence.

Discussion

In our previous study, the signaling pathways of JNK and Akt were shown to be important for establishment of persistent SARS-CoV infection, when these inhibitors were added soon after SARS-CoV infection [7]. Approximately 95% of confluent Vero E6 cells died 2 days after infection with SARS-CoV. The remaining 5% of cells that survived grew with persistent virus infection. When 24-well plates were used for experiments, the persistently infected cells reached confluence by 7 days. Interestingly, the PI3K/Akt inhibitor, LY294002, permitted cell survival when added after apoptotic events, but activation of JNK was also necessary for survival after apoptotic events. Our previous study demonstrated the importance of Akt activation for proliferation of SARS-CoV-infected cells [4]. Phosphorylation of Akt was down-regulated in subconfluent cells by SARS-CoV infection [13]. Nevertheless, LY294002-treated surviving cells that had escaped from SARS-CoV-induced apoptosis could still grow slowly. One of the reasons for this is that PI3K/Akt inhibitor needs 3 days after treatment to inhibit cell proliferation [13]. Therefore, persistent cell colonies may grow slightly in the presence of LY294002. SARS-CoV replicates in surviving cells, and these cells are still alive in the presence of LY294002, suggesting that the signaling pathway of PI3K/Akt is not necessary to prevent apoptosis in cells with persistent virus infection. The apoptotic signaling pathways may be blocked independent of PI3K/Akt in surviving cells. In this study, we demonstrated that the anti-apoptotic proteins Bcl-2 and Bcl-xL were present at elevated levels in persistently infected cells. Because Bcl-2 is slightly increased and phosphorylated at acute infection (24 h.p.i.), but not Bcl-xL (data not shown), Bcl-xL may be more important than Bcl-2 for survival. These results indicated that the PI3K/Akt signaling pathway is important for cell survival in the early stages of SARS-CoV-induced apoptosis, whereas the JNK, Bcl-2, and Bcl-xL pathways are important after apoptotic events. We found SP600125 that slightly prevented SARS-CoV-induced apoptosis (unpublished data). The JNK signaling pathway is one of the key factors for understanding persistence of SARS-CoV.

Interestingly, when we used the N expression system of vaccinia virus (DIs-N), Akt and JNK were phosphorylated in Vero E6. The differences in the results between our study and that reported by Surjit et al. using COS-1 are most likely due to the use of different cell cultures and different expression systems [15]. It is not yet clear whether N protein alone is able to induce phosphorylation of these signaling pathways in Vero E6 cells because we have no useful system for plasmid transfection of these cells. Both Akt and JNK were phosphorylated in our system due to additional stress by expression of vaccinia viral proteins. Because Bcl-2 and Bcl-xL were not increased by N protein expression, these anti-apoptotic proteins may not be downstream of Akt and JNK signaling pathways.

In this paper, we showed possible mechanisms of establishment of persistent SARS-CoV infection. Further investigations are necessary to determine signaling pathways, which are able to up-regulate Bcl-2 and Bcl-xL levels.

Acknowledgments

We thank Drs. S. Harada (National Institute of Infectious Diseases, Japan) and M. Funaba (Azabu University, Japan) for helpful suggestions. We also thank Ms. M. Ogata (National Institute of Infectious Diseases, Japan) for her assistance. This work was supported in part by the Japan Health Science Foundation and, Japan Society for the Promotion of Science, Tokyo, Japan.

References

[1] M.A. Marra, S.J. Jones, C.R. Astell, R.A. Holt, A. Brooks-Wilson, Y.S. Butterfield, J. Khattra, J.K. Asano, S.A. Barber, S.Y. Chan, A. Cloutier, S.M. Coughlin, D. Freeman, N. Girn, O.L. Griffith, S.R. Leach, M. Mayo, H. McDonald, S.B. Montgomery, P.K. Pandoh, A.S. Petrescu, A.G. Robertson, J.E. Schein, A. Siddiqui, D.E. Smailus, J.M. Stott, G.S. Yang, F. Plummer, A. Andonov, H. Artsob, N. Bastien, K. Bernard, T.F. Booth, D. Bowness, M. Czub, M. Drebot, L. Fernando, R. Flick, M. Garbutt, M. Gray, A. Grolla, S. Jones, H. Feldmann, A. Meyers, A. Kabani, Y. Li, S. Normand, U. Stroher, G.A. Tipples, S. Tyler, R. Vogrig, D. Ward, B. Watson, R.C. Brunham, M. Krajden, M. Petric, D.M. Skowronski, C. Upton, R.L. Roper, The genome sequence of the SARS-associated coronavirus, Science 300 (2003) 1399–1404.

[2] P.A. Rota, M.S. Oberste, S.S. Monroe, W.A. Nix, R. Campagnoli, J.P. Icenogle, S. Penaranda, B. Bankamp, K. Maher, M.H. Chen, S. Tong, A. Tamin, L. Lowe, M. Frace, J.L. DeRisi, Q. Chen, D. Wang, D.D. Erdman, T.C. Peret, C. Burns, T.G. Ksiazek, P.E. Rollin, A. Sanchez, S. Liffick, B. Holloway, J. Limor, K. McCaustland, M. Olsen-Rasmussen, R. Fouchier, S. Gunther, A.D. Osterhaus, C. Drosten, M.A. Pallansch, L.J. Anderson, W.J. Bellini, Characterization of a novel coronavirus associated with severe acute respiratory syndrome, Science 300 (2003) 1394–1399.

[3] T. Mizutani, S. Fukushi, M. Saijo, I. Kurane, S. Morikawa, Phosphorylation of p38 MAPK and its downstream targets in SARS coronavirus-infected cells, Biochem. Biophys. Res. Commun. 319 (2004) 1228–1234.

[4] T. Mizutani, S. Fukushi, M. Saijo, I. Kurane, S. Morikawa, Importance of Akt signaling pathway for apoptosis in SARS-CoV-infected Vero E6 cells, Virology 327 (2004) 169–174.

[5] T. Mizutani, S. Fukushi, M. Murakami, T. Hirano, M. Saijo, I. Kurane, S. Morikawa, Tyrosine dephosphorylation of STAT3 in SARS coronavirus-infected Vero E6 cells, FEBS Lett. 577 (2004) 187–192.

[6] T. Mizutani, S. Fukushi, M. Saijo, I. Kurane, S. Morikawa, Regulation of p90RSK phosphorylation by SARS-CoV infection in Vero E6 cells, FEBS Lett. 580 (2006) 1417–1424.

[7] T. Mizutani, S. Fukushi, M. Saijo, I. Kurane, S. Morikawa, JNK and PI3k/Akt signaling pathways are required for establishing persistent SARS-CoV infection in Vero E6 cells, Biochem. Biophys. Acta 1741 (2005) 4–10.

[8] P.K. Chan, K.F. To, A.W. Lo, J.L. Cheung, I. Chu, F.W. Au, J.H. Tong, J.S. Tam, J.J.J. Sung, H.K. Ng, Persistent infection of SARS coronavirus in colonic cells in vitro, J. Med. Virol. 74 (2004) 1–7.

[9] G. Palacios, O. Jabado, N. Renwick, T. Briese, W.I. Lipkin, Severe acute respiratory syndrome coronavirus persistence in Vero cells, Chin. Med. J. (Engl.) 118 (2005) 451–459.

[10] M. Yamate, M. Yamashita, T. Goto, S. Tsuji, Y.G. Li, J. Warachit, M. Yunoki, K. Ikuta, Establishment of Vero E6 cell clones persistently infected with severe acute respiratory syndrome coronavirus, Microbes Infect. 7 (2005) 1530–1540.

[11] K. Ishii, H. Hasegawa, N. Nagata, M. Mizutani, S. Morikawa, T. Suzuki, F. Taguchi, M. Tashiro, T. Takemori, T. Miyamura, Y. Tsunetsugu-Yokota, Induction of protective immunity against severe acute respiratory syndrome coronavirus (SARS-CoV) infection using highly attenuated recombinant vaccinia virus DIs, Virology (in press).

[12] E. Everitt, C. Wohlfart, Spectrophotometric quantitation of anchorage-dependent cell numbers using extraction of naphthol blue-black-stained cellular protein, Anal. Biochem. 162 (1987) 122–129.

[13] T. Mizutani, S. Fukushi, D. Iizuka, O. Inanami, M. Kuwabara, H. Takashima, H. Yanagawa, M. Saijo, I. Kurane, S. Morikawa, Inhibition of cell proliferation by SARS-CoV infection in Vero E6 cells, FEMS Immunol. Med. Microbiol. 46 (2006) 236–243.

[14] R. Kim, Unknotting the roles of Bcl-2 and Bcl-xL in cell death, Biochem. Biophys. Res. Commun. 333 (2005) 336–343.

[15] M. Surjit, B. Liu, S. Jameel, V.T. Chow, S.K. Lal, The SARS coronavirus nucleocapsid protein induces actin reorganization and apoptosis in COS-1 cells in the absence of growth factors, Biochem. J. 383 (2004) 13–18.

Available online at www.sciencedirect.com
SCIENCE DIRECT
ELSEVIER
Virology 351 (2006) 368–380
VIROLOGY
www.elsevier.com/locate/yviro

Induction of protective immunity against severe acute respiratory syndrome coronavirus (SARS-CoV) infection using highly attenuated recombinant vaccinia virus DIs

Koji Ishii[a], Hideki Hasegawa[b], Noriyo Nagata[b], Tetsuya Mizutani[c], Shigeru Morikawa[c], Tetsuro Suzuki[a], Fumihiro Taguchi[d], Masato Tashiro[d], Toshitada Takemori[e], Tatsuo Miyamura[a], Yasuko Tsunetsugu-Yokota[e,*]

[a] *Department of Virology II, National Institute of Infectious Diseases, Toyama, Shinjuku-ku, Tokyo 162-8640, Japan*
[b] *Department of Pathology, National Institute of Infectious Diseases, Gakuen, Musashimurayama-shi, Tokyo 208-001, Japan*
[c] *Department of Virology I, National Institute of Infectious Diseases, Gakuen, Musashimurayama-shi, Tokyo 208-001, Japan*
[d] *Department of Virology III, National Institute of Infectious Diseases, Gakuen, Musashimurayama-shi, Tokyo 208-001, Japan*
[e] *Department of Immunology, National Institute of Infectious Diseases, Toyama, Shinjuku-ku, Tokyo 162-8640, Japan*

Received 22 December 2005; returned to author for revision 9 March 2006; accepted 10 March 2006
Available online 6 May 2006

Abstract

SARS-coronavirus (SARS-CoV) has recently been identified as the causative agent of SARS. We constructed a series of recombinant DIs (rDIs), a highly attenuated vaccinia strain, expressing a gene encoding four structural proteins (E, M, N and S) of SARS-CoV individually or simultaneously. These rDIs elicited SARS-CoV-specific serum IgG antibody and T-cell responses in vaccinated mice following intranasal or subcutaneous administration. Mice that were subcutaneously vaccinated with rDIs expressing S protein with or without other structural proteins induced a high level of serum neutralizing IgG antibodies and demonstrated marked protective immunity against SARS-CoV challenge in the absence of a mucosal IgA response. These results indicate that the potent immune response elicited by subcutaneous injection of rDIs containing S is able to control mucosal infection by SARS-CoV. Thus, replication-deficient DIs constructs hold promise for the development of a safe and potent SARS vaccine.

Keywords: Vaccinia virus; Vaccine; SARS

Introduction

Severe acute respiratory syndrome (SARS) has become a priority for healthcare agencies around the world given its communicability, associated mortality, and the potential for pandemic spread. As of 31 July 2003, 8,098 SARS cases had been identified worldwide, resulting in 774 deaths and a mortality rate of about 9.6% (World Health Organization statistics). SARS is now known to result from infection with a novel coronavirus (SARS-CoV) (Drosten et al., 2003; Ksiazek et al., 2003; Peiris et al., 2003). Evidence that SARS-CoV is the etiologic agent of SARS follows an experimental infection of macaques (*Macaca fascicularis*), fulfilling Koch's postulates (Fouchier et al., 2003). The clinical manifestations of SARS are hardly distinct from other common respiratory viral infections, including influenza. Because influenza epidemics might occur simultaneously with the eventual re-emergence of SARS, an effective SARS vaccine is urgently required, as well as more sensitive diagnostic tests specific for SARS.

Structural characterization of SARS-CoV and characterization of its complete RNA genome (Marra et al., 2003; Rota et al., 2003; Ruan et al., 2003) have provided us with the opportunity to develop a SARS vaccine. Like other coronaviruses, SARS-CoV is a plus-stranded RNA virus with a 30-kb genome encoding replicase gene products and the 4 structural proteins; i.e., spike (S), envelope (E), membrane (M), and nucleocapsid

* Corresponding author. Fax: +81 3 5285 1150.
E-mail address: yyokota@nih.go.jp (Y. Tsunetsugu-Yokota).

0042-6822/$ - see front matter © 2006 Elsevier Inc. All rights reserved.
doi:10.1016/j.virol.2006.03.020

(N) (Marra et al., 2003; Rota et al., 2003). The S protein is thought to be involved in receptor binding, while the E protein has a role in viral assembly, the M protein is important for virus budding, and the N protein has a role in viral RNA packaging (for review, see reference (Holmes, 2003)). Recently, angiotensin-converting enzyme 2 (ACE2) has been identified as a cellular receptor for SARS-CoV (Li et al., 2003). Thus, the first step of infection likely involves binding of S protein to the ACE2 receptor. In a model of MHV infection, S protein is known to contain important virus-neutralizing epitopes that elicit neutralizing antibody responses in mice (Collins et al., 1982). Therefore, the S protein of coronavirus might be manipulated to induce immunity. However, S, M, and N proteins are also known to contribute to the host immune response (Anton et al., 1996; Jackwood and Hilt, 1995). A DNA vaccine encoding the S glycoprotein of the SARS-CoV induces T cell and neutralizing antibody responses, as well as protective immunity, in a mouse model (Yang et al., 2004). Vaccination with a plasmid expressing N protein is capable of generating strong N-specific humoral and T-cell-mediated immune responses in vaccinated C57BL/6 mice (Kim et al., 2004; Zhao et al., 2005; Zhu et al., 2004). In addition, N-specific $CD8^+$ T cells provide protective immunity against some coronaviruses (Collisson et al., 2000; Seo et al., 1997).

The DIs strain is a highly restricted host range mutant of the vaccinia virus isolated by successive 1-day egg passage of the DIE vaccinia strain, an authorized strain for smallpox vaccine and actually used in Japan until 1981. DIs does not replicate and is not pathogenic in mice, guinea pigs or rabbits. Furthermore, the DIs does not replicate in various mammalian cell lines (Tagaya et al., 1961). Recently, we established a system for foreign gene expression by inserting target genes into this strain, after which expression of (i) bacteriophage T7 polymerase, and (ii) the full-length HIV-1_{NL432} *gag* gene, was observed (Ishii et al., 2002), thus demonstrating the usefulness of this system.

In the present study, we constructed a recombinant vaccinia virus DIs expressing one or more SARS-CoV structural proteins (E, M, N, and S, or a combination of E, M, and S (E/M/S), or E, M, N and S (E/M/N/S)). These rDIs vaccines were administered to mice either subcutaneously or intranasally, and the humoral and cellular immunity against SARS-CoV in vaccinated mice were analyzed. We demonstrated here that replication-deficient DIs constructs expressing S protein alone or in combination with other components, but not N alone, elicited strong protective immune responses against SARS-CoV infection.

Results

Expression of SARS-CoV structural proteins by rDIs

The structures of transfer vectors used in this study (pDIsSARS-E, pDIsSARS-M, pDIsSARS-N, pDIsSARS-S, pDIsSARS-E/M, pDIsSARS-E/M/S and pDIsSARS-E/M/N/S) were summarized in Fig. 1. Expression of SARS-CoV N and S proteins in chick embryo fibroblast (CEF) cells infected

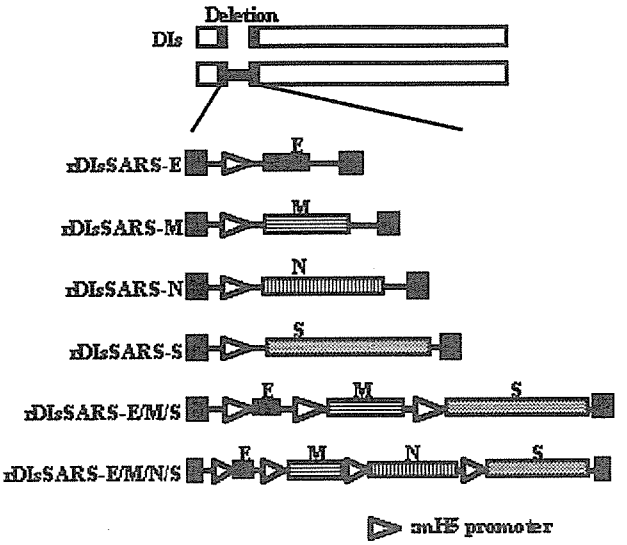

Fig. 1. Schematic diagram of rDIs constructs expressing SARS-CoV structural proteins. DNA fragments encoding E, M, N and S proteins were inserted into the location of the 15.4 kb deletion in DIs using the vaccinia virus transfer vector pDIsgptmH5. Six rDIs constructs are shown.

with rDIsSARS was detected by Western blotting using monoclonal antibodies (Fig. 2A) (Ohnishi et al., 2005). Purified SARS-CoV virion was used as a positive control (Fig. 2A, lane PC). A robust signal was detected at 50 kDa, corresponding to the N protein of SARS-CoV, as predicted by its genomic size (Marra et al., 2003; Rota et al., 2003). A band approaching 200 kDa likely corresponds to the S protein, which is known to be heavily glycosylated (Fig. 2A). Our results are consistent with data reported by Xiao et al. (2003) who expressed the full-length S glycoprotein of SARS-CoV Tor2 strain in 293 cells and demonstrated a protein approaching 180–200 kDa by SDS gel electrophoresis. Concerning the M protein, only a smear band in the stacking gel was detected using a polyclonal antibody against synthetic peptide of the M protein (Mizutani et al., 2004), presumably because it formed large oligomers with SDS-resistance in cells (Fig. 2A). Similar result was mentioned by the analysis of the M protein of SARS-CoV (Buchholz et al., 2004) and infectious bronchitis virus (Weisz et al., 1993).

The subcellular localization of S, M, and N proteins was analyzed by immunofluorescence staining. Cells infected with rDIsSARS-M demonstrated M proteins primarily co-localized with the Golgi marker GM-130 (Fig. 2B), which is consistent with the results of the recent study (Nal et al., 2005). Individually expressed SARS-CoV N protein could be detected partially with Golgi apparatus, but remained principally localized to the cytoplasm (Fig. 2B). Overexpressed recombinant SARS-S glycoprotein could be detected partially with Golgi apparatus, but also be detected throughout the cytoplasm (Fig. 2B). These results indicate that cells infected with rDIsSARS expressed significant levels of SARS-CoV proteins under the control of mH5 promoter with an expected post-translational processing (Nal et al., 2005; You et al., 2005).

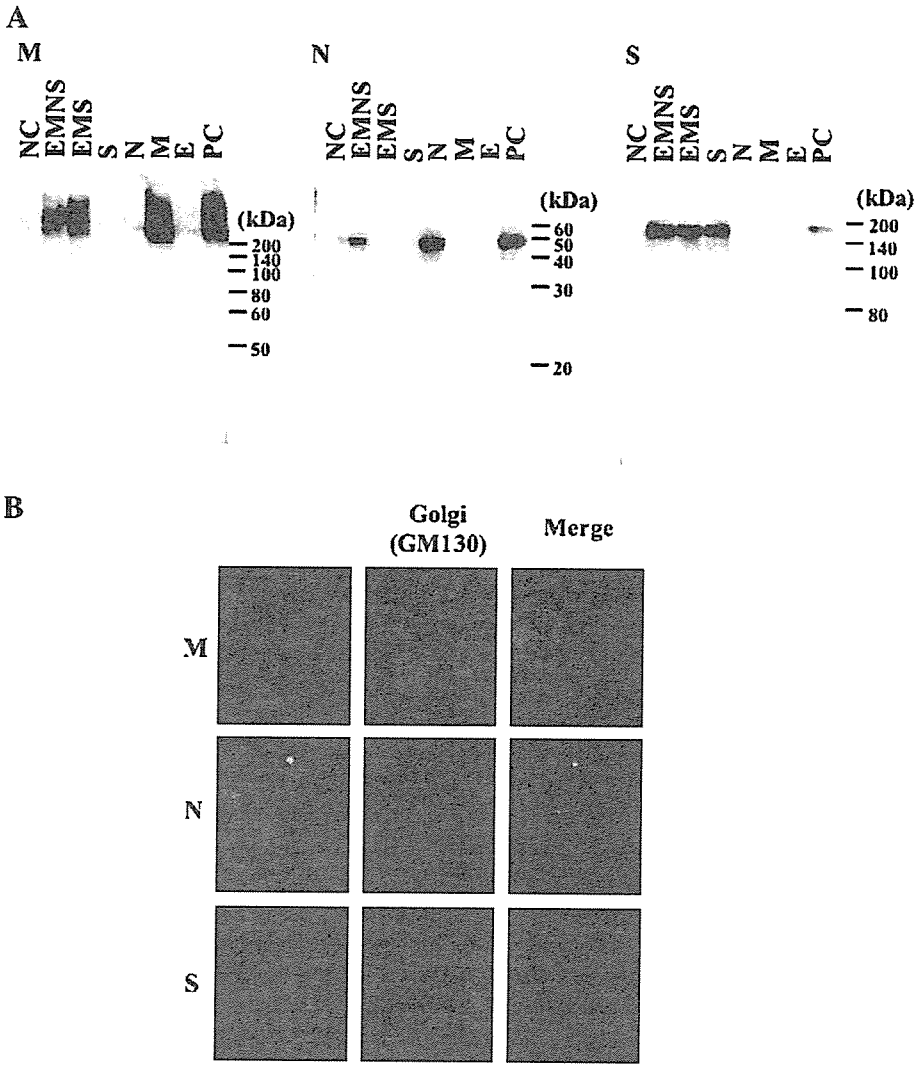

Fig. 2. Western blot analysis and indirect immunofluorescence analysis. (A) CEF cells were infected with rDIs constructs expressing SARS-CoV structural proteins (M, N and S, respectively). Purified SARS-CoV virion (0.5 μg) was used as a positive control. SARS-CoV proteins were detected using monoclonal antibodies (N and S) or polyclonal antibodies (M). Detection of bound antibodies was done with horseradish peroxidase-conjugated goat anti-mouse or anti-rabbit antibody, and visualized by chemiluminescence. (B) CEF cells were infected with rDIs constructs expressing SARS-CoV structural proteins (M, N and S, respectively). To detect SARS-CoV proteins, the cells were incubated with rabbit polyclonal antibodies against these proteins. The cells were further incubated with FITC-conjugated goat anti-rabbit IgG. To analyze subcellular localization of these proteins, monoclonal antibody against GM-130 (Golgi marker) and rhodamine-conjugated goat anti-mouse IgG were used. SARS proteins are shown in green, Golgi apparatus is shown in red and co-localization, where it occurs, is shown in yellow.

rDIsSARS induces serum IgG antibody responses specific for SARS-CoV

To examine the anti-SARS-CoV response in mice after inoculation with rDIsSARS, four mice in each group were subcutaneously or intranasally inoculated three times with 10 pfu of rDIsSARS-N, rDIsSARS-M, rDIsSARS-S, rDIs-SARS-E/M/S or rDIsSARS-E/M/N/S. Ten days after the final inoculation, vaccinated mice were observed to have high levels of anti-SARS-CoV IgG antibodies in their sera (Fig. 3).

In order to prove effective vaccination, we next examined whether neutralizing antibodies against SARS-CoV were elicited in these mice. Neutralizing antibodies against SARS-CoV were induced in mice following subcutaneous or intranasal injection of rDIsSARS-S, rDIsSARS-E/M/S, or rDIsSARS-E/M/N/S, but not in mice immunized with rDIsSARS-N or rDIsSARS-M. These results of ELISA data were incorporated into Fig. 3 by depicting the neutralization positive serum as closed circles. Thus, our results, consistent with others (Bisht et al., 2004; Buchholz et al., 2004; Yang et al., 2004), indicate that the S protein is a prerequisite for eliciting a sufficient IgG antibody response for neutralization. Similar neutralizing activity was obtained in mice receiving S alone or in combination with other components. Therefore, we expected that the rDIsSARS expressing E/M/N/S proteins in combination could be the best vaccine candidate among others.

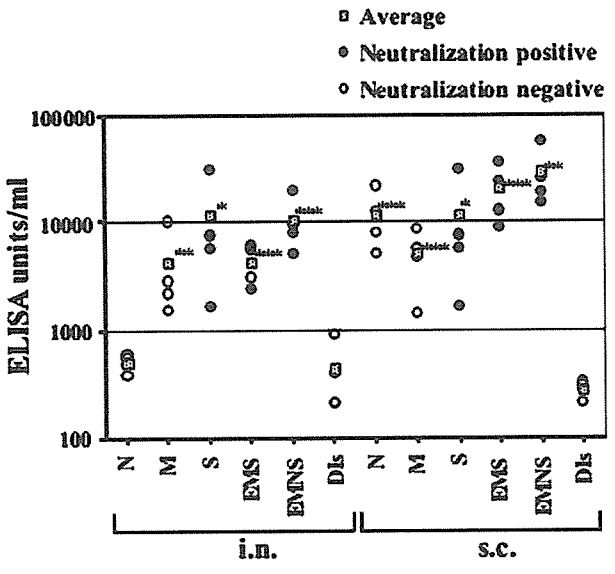

Fig. 3. Detection of anti-SARS-CoV IgG in vaccinated mice. IgG antibody levels against SARS-CoV were determined as described in Materials and methods. SARS-CoV-specific IgG titers were calculated as follows: SARS-specific IgG titer (ELISA units/ml) = (the unit value obtained for wells coated with virus-infected cell lysate) − (the unit value obtained for wells coated with non-infected cell lysate). $*P < 0.1$, $**P < 0.05$, $***P < 0.01$ vs. DIs-administered group. The data for neutralizing sera are represented by closed circles and the data for non-neutralizing sera are represented by open circles.

Intranasal inoculation of rDIsSARS expressing E/M/N/S induces SARS-CoV-specific IgA in nasal mucosa and a high level of mucosal IgG in parallel with that of serum IgG

Mucosal IgA response is believed to be crucial for the protective immunity against various pathogens (Meeusen et al., 2004). We, next, examined mucosal immunity in the respiratory tracts of mice inoculated with rDIsSARS either subcutaneously or intranasally. The level of anti-SARS-CoV IgA within nasal wash fluid of vaccinated mice was determined by enzyme-linked immunosorbent assay (ELISA). As shown in Fig. 4A, substantial levels of anti-SARS-CoV IgA were detected only in mice received intranasal inoculation of rDIsSARS-E/M/N/S, compared to those inoculated with parental DIs ($P = 0.0010$). The level of IgA detected in intranasally rDIsSARS-E/M/N/S-inoculated mice was similar to that observed following intranasal immunization with UV-inactivated, purified SARS-CoV virion (positive control). On the other hand, subcutaneous injection of all forms of rDIsSARS produced only slightly higher levels of IgA than those observed in DIs -injected control mice. Therefore, the results indicated that the subcutaneous route of injection is inefficient, especially when mucosal IgA response is required.

Since neutralizing activity was, nevertheless, detected in the nasal washes of mice following subcutaneous immunization (data not shown), we also measured anti-SARS-CoV IgG levels in the nasal washes of these mice (Fig. 4B). High levels of IgG were detected in the nasal washes of mice following nasal immunization, which were observed to correspond well with IgG levels in the serum (Fig. 4C). A similar trend was observed in mice following subcutaneous immunization, despite at a lower level than in mice immunized intranasally. These results suggest that neutralizing IgG antibodies are capable of reaching the mucosal surface if plasma levels are high enough.

Protection of rDIsSARS-immunized mice from nasal SARS-CoV challenge is achieved without mucosal IgA response

The level of protection against SARS-CoV challenge in mice following inoculation with rDIsSARS is a critical issue for the vaccine development. We inoculated three times with 10 pfu of rDIsSARS-N, rDIsSARS-E/M/S or rDIsSARS-E/M/N/S into four mice in each group either subcutaneously or intranasally. One week after final inoculation, the mice were challenged intranasally with 10^4 tissue culture 50% infectious dose ($TCID_{50}$) of SARS-CoV. The results were shown in Fig. 4D. In mice inoculated with saline, 10^3 $TCID_{50}$/ml of SARS-CoV were recovered from lung wash fluid on day 3. In contrast, titers of SARS-CoV from the lungs of mice subcutaneously immunized with rDIsSARS-E/M/S or rDIsSARS-E/M/N/S were below the limits of detection. The same was true for mice intranasally immunized with rDIsSARS-E/M/N/S, whereas the virus was recovered in mice similarly immunized with rDIsSARS-E/M/S. Taken into consideration of a relatively low or marginal level of mucosal IgA antibody in mice intranasally immunized with rDIsSARS-E/M/N/S or rDIsSARS-E/M/S, or even no IgA response by subcutaneous route as described above, it was suggested that mucosal IgG antibody, but not IgA antibody, likely contributed to the protective immunity, especially in mice simultaneously immunized with recombinant rDIsSARS-E/M/N/S.

On the other hand, titers of SARS-CoV from the lung wash fluid of mice intranasally or subcutaneously immunized with rDIsSARS-N, were similar or slightly lower than the titers of negative controls, suggesting that intranasal or subcutaneous administration of rDIsSARS-N does not protect mice from SARS-CoV challenge, which is highly reflected by the non-neutralizing nature of anti-SARS-CoV N antibodies.

Cellular immunity induced by rDIsSARS

Although now we know that the systemic neutralizing IgG antibody against SARS-CoV S protein is a major component of protective immunity, T cell responses are also important to protect hosts from various viral infection. In a previous study of coronaviruses, S protein was shown to play an important role in viral pathogenesis, as well as induction of protective immunity (Holmes, 2003). In order to assess the ability of rDIsSARS to induce SARS-CoV S-specific T cells, T cells from axillary lymph nodes (ALN), superficial cervical lymph nodes (CLN) and spleens of mice subcutaneously immunized with rDIs-SARS-S or DIs were isolated and stimulated in vitro with UV-inactivated, purified SARS-CoV virion. Culture supernatant was collected 4 days later, and the levels of interferon-γ (IFN-γ), interleukin (IL)-2, IL-4, IL-5 and tumor necrosis factor-α (TNF-α) were measured. T cells in ALN produced the greatest cytokine levels (Fig. 5, and data not shown). This is not surprising in light of the subcutaneous route of immunization.